Addis Ababa Institute of Technology

School of Mechanical and Industrial Engineering

# Cost-of-energy optimization of 3D printed small-scale wind turbine blades

A Thesis Submitted to the School of Mechanical and Industrial Engineering,
Addis Ababa Insititute of Technology

Presented in partial fulfillment for the Degree of Master of Science in Mechanical Engineering (Thermal Engineering)

Prepared by: Abraham Kassahun Negash

Advisor: Dr. Ing. Wondwossen Bogale

Addis Ababa University
Addis Ababa, Ethiopia
June 2024


Addis Ababa Institute of Technology

School of Mechanical and Industrial Engineering

# Cost-of-energy optimization of 3D printed small-scale wind turbine blades

By

Abraham Kassahun Negash

Approved by the Board of Examiners:

| | | |
|---|---|---|
| Dr. Ing. Wondwossen Bogale<br>Advisor | _____<br>Signature | _____<br>Date |
| Dr. Abdulkadir Aman<br>Examiner | _____<br>Signature | _____<br>Date |
| Dr. Tilahun Nigussie<br>Examiner | _____<br>Signature | _____<br>Date |
| Dr. Araya Abera<br>School Dean | _____<br>Signature | _____<br>Date |
| Dr. Sosina Mengistu<br>Associate Director for PG Program | _____<br>Signature | _____<br>Date |

## Declaration

I hereby declare that the work which is being presented in this thesis entitled “Cost-of-energy optimization of 3D printed small-scale wind turbine blades” is an original work of my own, has not been presented for a degree of any other university and all the resource of materials used for this thesis have been duly acknowledged.

_____ _____

Abraham Kassahun Negash Date

This is to certify that the above declaration made by the candidate is correct to the best of my knowledge.

_____ _____

Dr. Ing. Wondwossen Bogale (Advisor) Date

# Table of Contents

Acknowledgment....iv
Abstract....v
Chapter 1. Introduction....1
1.1. Background of the Study....1
1.2. Problem Statement....3
1.3. Objectives....4
1.3.1. Main Objectives....4
1.3.2. Specific Objectives....4
1.4. Scope....5
Chapter 2. Literature Review....6
2.1. World Energy Scenario....6
2.2. Ethiopian Energy Scenario....8
2.3. History of Wind Turbines....9
2.4. Wind Resource Assessment....11
2.5. Types of Wind Turbines....12
2.6. Components of Small Horizontal Axis Wind Turbines....16
2.6.1. Blade....16
2.6.2. Generator....16
2.6.3. Tower....17
2.6.4. Speed Control System....19
2.6.5. Yaw Control System....20
2.7. Design of Small Wind Turbine Blades....20
2.7.1. Important Parameters....20
2.7.2. Momentum Theory and the Betz Limit....22
2.7.3. Aerodynamics of Wind Turbine Blades....22
2.7.4. Blade Element Momentum Calculations....26
2.7.5. Structural Analysis of Wind Turbines....29
2.8. Manufacturing of Small Wind Turbine Blades....30
2.8.1. Conventional Manufacturing....30
2.8.2. Additive Manufacturing....32
2.9. Cost Modeling of Wind Turbines....35
2.10. Optimization of Wind Turbines....36
Chapter 3. Methodology....38
3.1. Overview....38
3.2. Additive Manufacturing Cost Modeling....40
3.2.1. Definition of Scope....40
3.2.2. Build Time Estimation....40
3.2.3. Indirect Cost Rate....43
3.2.4. Direct costs....44
3.2.5. Pre-processing cost....44
3.2.6. Post-processing cost....44
3.2.7. Virtual Factory....45
3.2.8. 3D Printer Specifications....45
3.2.9. 3D Printing Process Parameters....46
3.2.10. Cost of Other Components....48
3.3. Benchmark design....48
3.4. Airfoil Polar Data Collection....49
3.5. Optimization Program....50

3.5.1. Creating a Population of Designs....51
3.5.2. Analyzing Designs....51
3.5.3. Selection and Crossover....53
3.5.4. Mutation....53
Chapter 4. Results and Discussion....56
4.1. Optimization Results....56
4.2. Discussion....57
4.3. Sensitivity Analysis....58
Chapter 5. Conclusion....60
References....62
Appendix....68
Appendix A: Source code....68
Parameters.py....68
cost_model.py....69
windspeed_pd.py....70
BEM_Re_intrp.py....70
Config.py....78
Population.py....80
Main.py....82

# Table of Figures

Table 2.1: Completed and upcoming wind projects in Ethiopia (Dingeto Hailu et al., 2021)....9
Table 2.2: IEC turbine classes (*Wind Turbines. Part 2, Small Wind Turbines*, 2013)....29
Table 2.3: design load cases of the simple load model (*Wind Turbines. Part 2, Small Wind Turbines*, 2013)....30
Table 3.1: Parameters used in cost modeling....47
Table 4.1: Input parameters of the optimization....56
Table 4.2: Result parameters of the optimized design....56
Table 4.3: Results of sensitivity analysis....59

# Table of Figures

Figure 2.1: Annual Global Energy Consumption in EJ (1800 – 2022) (Ritchie et al., 2022)....6
Figure 2.2: Share of Global Primary Energy (Energy Institute, 2023)....8
Figure 2.3: Vertical-axis wind turbine rotor concepts; Savonius rotor (left), Darrieus rotor (center), and H-rotor (right) (Hau & Hau, 2006)....13
Figure 2.4: Various alternative wind turbine concepts (Hau & Hau, 2006)....15
Figure 2.5: Twist and chord distribution of a blade (Akbari et al., 2022)....16
Figure 2.6: Different types of towers: Monopole tower (left), lattice tower (top right), and guyed tower (bottom right) (Westwood, 2012; Wood, 2011)....18
Figure 2.7: Idealized flow through an actuator disc according to momentum theory (Hau & Hau, 2006)....22
Figure 2.8: Lift, drag, and relative wind speed at a blade section....23
Figure 2.9: Annular streamtube (Wood, 2011)....26
Figure 2.10: VARTM process (Wood, 2011)....31
Figure 2.11: The adopted XZERES 442SR wind turbine (above) and the 3D printed blade sections (below) (B. K. Post et al., 2018)....32
Figure 2.12: Final molds produced, upper and lower sections (B. Post et al., 2017)....33
Figure 2.13: The 3D printer used (left) and the three methods used (right) (Poole & Phillips, 2015) ....34

Figure 2.14: 3D printed blades on an AIR-X generator (Akour et al., 2018).....34
Figure 3.1: Methodology flow chart.....39
Figure 3.2: The Ender 3 v2 3D printer.....46
Figure 3.3: The Skystream 3.7 (*Small Turbine Product Reviews*, n.d.).....49
Figure 3.4: Power curve of the Skystream 3.7 (*XzeresSkystream3.7_2.1kW_3.7 — NREL/Turbine-Models Power Curve Archive 0 Documentation*, n.d.).....49
Figure 3.5: Flowchart of genetic optimization algorithm.....51
Figure 3.6: Flow chart of the blade element momentum analysis program.....54
Figure 3.7: Flow chart of the blade element momentum analysis program (cont.).....55
Figure 4.1: A Rendering of the Design.....57

## Acknowledgment

I would like to thank my family for their support during the writing of this thesis. My sincerest thanks goes to my advisor Dr. Ing. Wondwossen Bogale for his useful follow up and advice. My thanks also goes out to Nathnael Bekele from SMiE staff for his advice. Additionally, I would like to thank my classmates and friends with whom I spoke to about this project on different occasions.

# Abstract

Human-induced climate change is an urgent challenge that necessitates the adoption of renewable energy sources. Wind energy conversion proves to be a promising option, with the horizontal axis wind turbines being identified as the most efficient and mature technology. While large turbines have been widely explored, there is a need for small-scale power solutions – notably in Ethiopia given its low electrification rate. The optimization of wind turbines is a well researched topic, but cost-of-energy optimization has been a challenge due to the difficulty in modeling the cost of traditional wind turbine manufacturing techniques. This research explores the use of 3D printing cost models to optimize energy costs in small-scale wind turbine blades. The cost involved in 3d printing a small wind turbine blade are explored. The cost of each activity in the process is modeled and a total cost estimate is stipulated. A linear relationship was found between the volume of the blade and the turbine cost. This relationship was used in the cost-of-energy optimization of the blade. A python code utilizing a genetic algorithm and a blade element momentum analysis model is written and utilized to obtain a cost-of-energy optimized design. The design variables chosen for optimization are the design wind speed, the tip-speed ratio and the airfoils used. The wind distribution was taken to be that of Addis Ababa. The results indicate the great potential of direct cost-of-energy optimization. A cost of energy of 0.67 $/KWh is obtained for the design which is better than the Skystream 3.7 wind turbine for our location. Sensitivity analysis is also performed by varying the design variables. The objective was found to be much more sensitive to the tip-speed ratio than the design wind speed.

# Chapter 1. Introduction

## 1.1. Background of the Study

Wind energy is one of the most promising renewable energy sources for meeting the increasing global demand for electricity. The cost of large on-shore wind energy has been decreasing and is currently competitive with that of conventional fossil fuels (*Renewable Power Remains Cost-Competitive amid Fossil Fuel Crisis*, 2022). For small-scale wind turbines, however, the cost is still comparatively high. For example, the levelized cost of electricity (LCoE) for residential wind turbines (<20kW) in the US was estimated to be 94 $/MWh under good wind conditions (9.52 m/s) (Vimmerstedt et al., 2022). To contrast, the LCoE for a combined cycle gas turbine in the US is 71 $/MWh (NEA, 2020).

Ethiopia has an installed wind energy capacity of 324 MW, which is much lower than its potential of 10 GW. Completed large wind turbine projects were Adama I (51 MW; 157 GWh/yr), Adama II (153 MW; 479 GWh/yr) and Ashegoda (120 MW; 450 GWh/yr), with a total capacity of 324 MW and an annual energy production of 1086 GWh. Upcoming projects include Ayisha (300 MW; 592 GWh/yr), Messobo (42 MW; 104 GWh/yr), Assela (100 MW; 197 GWh/yr) and Debre Birhan (100 MW; 197GWh/yr) which have grand total capacity of 866 MW and annual energy production of 2176 GWh. This is still a far cry from the estimated wind potential of 10 GW (Dingeto Hailu et al., 2021).

Most wind turbines in use are horizontal-axis wind turbines. These can be further classified into small-scale, small commercial, medium commercial and large commercial based on their rated power. Small-scale wind turbines typically produce less than 16 kW of electricity and generate more costly electricity than larger turbines, but can be an economically feasible power source in off-grid locations with good wind conditions (Tummala et al., 2016).

One alternative to exploit the still untapped wind potential of Ethiopia is by using small-scale wind turbines. A market assessment for locally manufactured small wind turbines (SWTs) in Ethiopia was commissioned by MercyCorps and carried out by Wind Empowerment, an association for the development of locally manufactured small wind turbines for sustainable rural electrification. The report explores the role of small wind turbines (SWTs) in electrifying remote communities in the Somali, Afar and Southern Oromia regions of Ethiopia, where only 1% of the rural population has access to electricity. The report compares SWTs with other off-grid power generation technologies using the levelized cost of energy (LCoE) as the key metric. The report also considers the costs and

benefits of local manufacture or importation of SWT components, as well as the installation and operation/maintenance of the systems. The report concludes that SWTs can play a role in rural electrification in Ethiopia, but they face challenges such as lack of data on wind potential, lack of skilled workforce, lack of financial incentives, and lack of regulatory framework (Eales et al., 2016).

The optimization of such systems is a necessity in order to achieve good performance. There are a few performance measures for wind turbines such as coefficient of power, annual energy production, and cost of energy (COE). Cost of energy compares turbine cost, balance of system costs and operational/maintenance costs to the annual energy production to measure how much a unit of energy costs. It strikes a balance between cost, aerodynamic performance and structural integrity which makes it an important metric (Andrew Ning et al., 2014). COE is essential in enabling the competitiveness of wind energy compared to nonrenewable sources and paving the way to its greater adoption, especially for small-scale wind turbines. For this metric to be useful, however, an accurate cost model must be used (Andrew Ning et al., 2014).

Manufacturing cost analysis can be performed using either cost estimators or cost models. Cost estimators provide a cost estimate without showing the interrelationship of relevant parameters. Cost models on the other hand do indicate the final cost estimate as well as the relationship between parameters. Both cost estimators and cost models are evaluated on the accuracy and consistency of their cost estimate (Bernard et al., 2019). One way to ensure the accuracy of the cost model is to use a manufacturing technique that can be reliably modeled.

3D printing, also known as additive manufacturing, is an emerging technology that enables the fabrication of complex shapes and structures with high precision and flexibility. 3D printing has been applied to various fields, such as aerospace, biomedical, and automotive engineering, due to its advantages over traditional manufacturing methods, such as reduced material waste, lower labor costs, and shorter production time. Recently, 3D printing has also been explored as a potential method for producing wind turbine blades, especially for small-scale applications (Bassett et al., 2015; Poole & Phillips, 2015). 3D printing can offer several benefits for wind turbine blade manufacturing, such as enabling customized designs, optimizing aerodynamic performance, and reducing environmental impact. In addition, its cost is relatively easy to model. However, 3D printing also poses some challenges and limitations, such as high material costs, low mechanical strength, and limited scalability. Therefore, there is a need for a comprehensive and systematic analysis of the feasibility and profitability of 3D printing for wind turbine blade production.

The aim of this study is to develop and experimentally validate a 3D printing cost model for the cost-of-energy optimization of small-scale wind turbine blades. We will consider various factors that affect the cost and performance of 3D printed wind turbine blades, such as material properties, printing parameters, blade geometry, and operating conditions. We will use a multi-objective optimization approach to find the optimal design solutions that minimize both the cost-of-energy and the levelized cost-of-energy of 3D-printed wind turbine blades. We will also conduct experimental tests to verify the accuracy and reliability of our 3D printing cost model and optimization results.

In this research, we first review the literature on 3D printing and wind turbine blade manufacturing, highlighting the main advantages and challenges of 3D printing for wind energy applications. Additionally, we review available literature on cost models for 3D printing. Then we describe the methods we used to develop our 3D printing cost model and optimization framework, including the assumptions, equations, and algorithms we employ. Next, we present the results of our optimization, showing the optimal design solutions and performance characteristics of 3D-printed wind turbine blades. Finally, we discuss the implications and limitations of our study, as well as suggestions for future research.

## 1.2. Problem Statement

As of 2017, 55.7 % of Ethiopians don't have access to a basic electricity supply, i.e. electric power enough to provide lighting to all members of the household and power additional devices such as a phone charger or a radio. Electrification is especially poor in rural areas where 70.8 % of households don't have access to a basic electricity supply (*Ethiopia - Multi-Tier Framework (MTF) Survey | Data Catalog*, n.d.). To address this problem, the National Electrification Program 2.0 has made it its mission to provide full electricity access to all Ethiopians by 2025 using 65 % grid solutions, and 35 % off-grid solutions (Ministry of Water, Irrigation, and Energy, 2019).

Wind energy has become increasingly popular with greater utilization of small wind for urban as well as off-grid applications. However, their prevalence is still relatively low with a capacity of a little more than 1 GW being installed globally at the end of 2017 (Tzen, 2020). Ethiopia has a vast potential for renewable energy, with abundant solar and wind resources that could make it economically feasible to develop optimized renewable energy-based electricity systems. In off-grid locations where there is an adequate wind resource, using wind energy can make a major difference in providing cheap and reliable electricity. Although much research has been conducted on small wind turbines' basic design configurations and component optimization, getting a good cost-of-

energy for most situations remains a challenge. The cost of energy of small wind turbines can vary between 10 c/kWh and 2 €/kWh. This variability is due to variation in the wind turbine's capacity factor, the annual mean wind speed of the site and the presence of economic incentives (Tzen, 2020).

Optimization of the cost of energy has been performed by a few studies (Andrew Ning et al., 2014; Maki et al., 2012). It is noteworthy that optimizations done on small wind turbines focus on aerodynamic and structural optimization. This is expected since no cost models for small wind turbines have been found and one cannot do a cost optimization without a cost model or estimator.

Furthermore, the cost models already in use for large wind turbines are based on traditional 2D laminate lay-up manufacturing for the composite components. These cost models are inaccurate as traditional 2D laminates have uncertainties when it comes to the labor and processes used. The models usually overestimate the cost (Chehouri et al., 2015).

Finally, it has been observed that site-specific designs reduce the cost of wind turbines by a significant amount (Fuglsang et al., 2002). Traditional composite manufacturing methods use molds, which must be made for each new design. It is therefore cost-prohibitive to tailor wind turbine to a specific wind distribution as the molds cannot be then reused.

To address these issues, this thesis proposes to employ 3D printing as the manufacturing process because it can offer reliable predictions by analyzing the model and its volume. Several publications have already looked at additive manufacturing cost models (Bernard et al., 2019; Busachi et al., 2017; Costabile et al., 2017; Ding et al., 2021; Kadir et al., 2020), but none have assessed their application to small-scale wind turbine blade optimization. In addition, the ability to 3D print any shape without the added mold costs makes it possible to utilize site-specific optimization cost-efficiently.

## 1.3. Objectives

### 1.3.1. Main Objectives

The main objective of this study is to perform a cost-of-energy optimization of a small-scale wind turbine blade with the aim of manufacturing it using 3D printing.

### 1.3.2. Specific Objectives

The specific objectives of the study are:

- Identifying the design variables to be used in optimization,

- Deriving the cost relationships of the 3D printing process,
- Developing an optimization algorithm based on the genetic algorithm and blade element momentum theory,
- Performing an evaluation of the optimal design variables, and
- Modeling of the 3D geometry using SolidWorks.

## 1.4. Scope

This study is concerned with cost of energy optimization of small wind turbine blades. Specifically, it seeks to exploit additive manufacturing to obtain an accurate cost model for their optimization.

A wind energy conversion system, besides the blades, contains the support structure, the gearbox and electrical generator, the control system and the energy storage system. Simple scaling models will be used to obtain the costs of these components and the detailed cost modeling will focus on the blade.

# Chapter 2. Literature Review

## 2.1. World Energy Scenario

Energy is one of the most important resources humans need to survive and flourish. Main turning points in human history like the discovery of fire, the domestication of animals, the industrial revolution, and the atomic age, were all instances of the utilization of new energy sources. Population increase and improvement of living standards have necessitated exponential increase in energy consumption. The total energy consumption has exploded from 20 EJ in 1800 to 644 EJ in 2022 as seen in figure 2.1 (*Ritchie et al., 2022*).

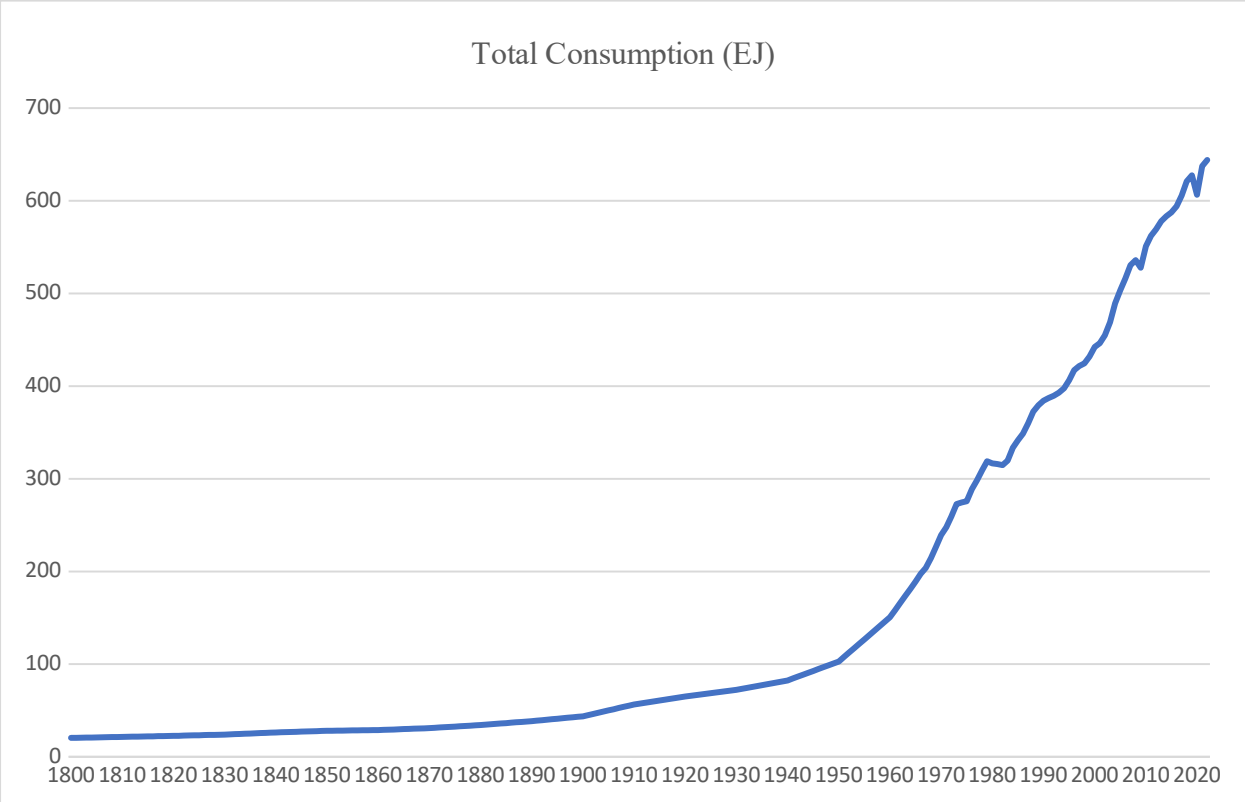


*Figure 2.1: Annual Global Energy Consumption in EJ (1800 – 2022) (Ritchie et al., 2022)*

There are several sources of energy in common use. In general, energy sources can be divided as primary and secondary sources of energy. Primary sources of energy are found in nature. These include fossil fuels like coal, oil, and natural gas, hydroelectricity, nuclear energy, solar energy, wind energy, biomass, geothermal energy, and tidal waves. Secondary sources of energy are processed from primary energy sources. Some examples of this are electricity and hydrogen.

Energy sources can also be renewable or non-renewable. Renewable energy sources are those that won't be depleted anytime soon. They are directly or indirectly related to the sun. Examples are solar energy, wind energy, hydroelectricity, and biomass. Non-renewable energy sources are

available in a fixed amount and are predicted to run out soon. In 2020 it was estimated that the proven deposits of coal will last 139 years, while oil and natural gas were estimated to last 57 and 49 years respectively at current rates of production (Energy Institute, 2023).

Besides the looming catastrophe of reliance on energy sources that can run out soon, there is also the issue of climate change to contend with. The burning fossil fuels has resulted in increased carbon dioxide in the atmosphere which has been linked to global warming, disruption of the global water cycle, increase in the frequency of extreme climate events, and sea level rise (Intergovernmental Panel On Climate Change, 2023). To address this, the most recent legally-binding agreement on climate change signed by 196 parties at the UN Climate Change Conference in Paris states that its signatories must limit global temperature increase below 2 °C above pre-industrial levels by the end of the century and pursue efforts to limit global temperature increase below 1.5 °C (UNFCC, 2015). It is worth noting that the current global temperature is already 1.1 °C greater than pre-industrial levels. To this end, the Intergovernmental Panel on Climate Change (IPCC) published a report on the effects of a 1.5 °C temperature rise. In this report it was mentioned that achieving net zero emissions by 2050 is an important step in reaching this goal (IPCC, 2018).

Figure 2.2 shows that the share of renewable energy in the global energy mix has been increasing and reached around 15% in 2022. While the share of oil has decreased, coal and natural gas have seen a slight increase over the past two decades (Energy Institute, 2023). If the goals set by the Paris Agreement are to be fulfilled, clearly more adoption of renewable energy sources is necessary.

As of 2021, the total installed capacity for wind energy is 743 GW helping to avoid the release of 1.1 billion tons of $CO_2$ annually. If the goal of staying below 2 °C temperature increase by the end of the century is to be realized, 180 GW of wind energy must be installed every year. If the further goal of achieving net zero emissions by 2050 is to be achieved, up to 280 GW of wind energy must be installed annually after 2030 (Bath, 2021).

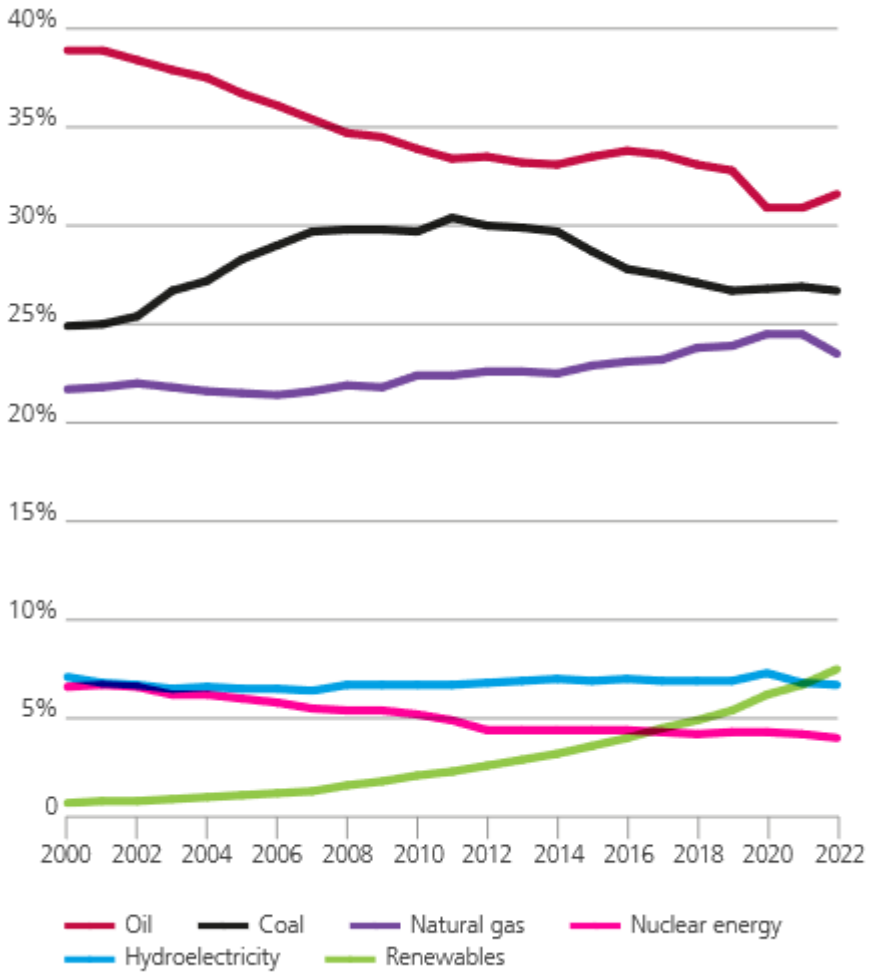


*Figure 2.2: Share of Global Primary Energy (Energy Institute, 2023)*

## 2.2. Ethiopian Energy Scenario

The total annual energy supply of Ethiopia is around 450,000 GWh. Of this total, 88% is supplied by renewable sources like wood, agricultural waste, hydro, and wind, 10% from oil, and 1% from coal and other sources. 96% of the energy from renewable sources is from biomass. When it comes to the generation of electricity, of the total 15,817 GWh produced in 2021, 94% was generated from hydroelectric, 5% from wind and the rest from solar and bioenergy (Energy Profile Ethiopia, 2023).

In 2021, most of the population in urban areas, 94.3%, was found to have access to electricity. However, only 42.8% of the rural population gets access to electricity (*World Bank Open Data*, n.d.). This segment of the population was estimated to be 77.3%. Due to the majority of this population not living near a grid, off-grid solutions like small wind can be a good alternative.

As was stated, the majority of the country's electricity is generated form hydroelectric dams. The Ethiopian Electric Power Corporation operates 22 power generating stations, 16 of them hydro.

Including the early generation units of the Grand Renaissance Dam, Ethiopia has a total hydoelectric installed capacity of 4,818.2 MW (*Power Generation – Eep*, n.d.).

Ethiopia also has an installed wind energy capacity of 404 MW which is a far cry from the country's total potential of 10 GW. Up till now, three wind farms have been completed; Ashegoda, Adama I and Adama II windfarms. Other windfarms are also in development in Ayisha, Messobo, Assela and Debre Birhan (Dingeto Hailu et al., 2021). All the main wind projects in Ethiopia are shown below in table 2.1.

*Table 2.1: Completed and upcoming wind projects in Ethiopia (Dingeto Hailu et al., 2021)*

| No. | Project | Capacity (MW) | Annual Energy Production (GWh) |
|---|---|---|---|
| Completed projects | | | |
| 1 | Adama I | 51 | 157 |
| 2 | Adama II | 153 | 479 |
| 3 | Ashegoda | 120 | 450 |
| | Total | 324 | 1086 |
| Upcoming projects | | | |
| 4 | Ayisha | 300 (currently generating 80 MW) | 592 |
| 5 | Messobo | 42 | 104 |
| 6 | Assela | 100 | 197 |
| 7 | Debre Birhan | 100 | 197 |
| | Grand Total | 866 | 2176 |

## 2.3. History of Wind Turbines

Wind power was routinely harnessed even before the industrial revolution. Sail ships used all over the world as well as wind mills for grinding grain are well-known applications. Other applications include sawing timber, pressing oil, shredding tobacco, and pumping water (Gipe & Möllerström, 2022).

In the late 19th century, the development of wind turbines began with the introduction of electricity. Scottish professor James Blyth, Charles De Goyon, and Charles Brush developed multi-bladed windmills, while Danish inventor Poul la Cour focused on four-bladed turbines. In the 1920s, several engineers contributed to the development of wind turbines, including Louis Constantin, Ludwig Prandtl, Kurt Bilau, Albert Flettner, and Georges Jean Marie Darrieus (Gipe & Möllerström, 2022).

Larger and larger wind turbines began to be built, with the Moscow Central Institute for Wind Energy installing the largest of its time in 1930. The 1 MW Smith-Putnam wind turbine in Vermont,

US, was two-bladed and 53 m in diameter. However, these were not durable machines (Gipe & Möllerström, 2022).

Ulrich Hütter, a German engineer, deduced that three is the optimal number of blades for turbines operating at tip speed ratios 4-7 and argued that a large number of medium-sized turbines is more economical than a few large ones. After WWII, Hütter built two notable turbines, the WE-10 and the StGW-34, with fiberglass as a blade material and the Hütter flange. Johannes Juul, a Danish contemporary of Hütter, combined fixed pitch stall regulation with pitch regulation using just the blade tips. His most successful designs were a 13-m diameter 65kW mill at Bogø and a 24-m diameter 200kW mill at Gedser, both of which were efficient and durable (Gipe & Möllerström, 2022).

In France, wind energy was gaining momentum with the construction of a 30 m diameter turbine with an 800 kW alternator. Neyrpic and Louis Vadot began testing wind turbines in 1958, producing 700,000 kWh of electricity from 1962 to 1966. In England, the British Electrical Authority funded three 100 kW projects in the Orkney islands, Wales, and the Isle of Man. The Orkney islands turbine had an 18.3 m diameter rotor rated at 13.4 m/s, while the Wales turbine was a pneumatic wind turbine first designed and tested by Jean-Edouard Andreau in France. The Isle of Man turbine produced 230,000-240,000 kWh/year during full operation (Gipe & Möllerström, 2022).

After the moon missions, NASA and large aerospace companies began working on larger wind turbines, but they were not as successful as expected. The Mod-0A saw some commercial success when Westinghouse installed 15 of their 600 kW turbines in Oahu. The Germans built the largest wind turbine yet, the Growian, but it was a failure costing twice its estimate and dismantled after only 420 hours of service. The Danish building upon Juul's Gedser mill built two 630 kW turbines, Nibe A and Nibe B, which were less expensive and operated for more hours (Gipe & Möllerström, 2023).

Danish wind turbines were built by individuals in response to Denmark's move towards nuclear energy. Christian Riisager built his own machine based on Juul's Gedser turbine and connected it to the grid. The Tvind turbine, built by students at Tvind School, was the largest and most successful of its time, featuring cantilevered blades and a 1 MW turbine with 27 m long blades. Grove-Neilsen began mass manufacturing these blades at Økaer, while Herborg Vindkraft used their blades and other off-the-shelf components to create the 30 kW HKV-10. The HKV-10 was bought by Vestas and modified into the popular V15 model. Other companies in the Danish wind turbine business included Danregn Vindkraft, later renamed Bonus, and Nordtank. The German company Siemens

bought Bonus, and later merged with Spanish wind turbine maker Gamesa to become Siemens Gamesa (Gipe & Möllerström, 2023).

After the second oil embargo in 1979, California introduced subsidies for renewable energy and made wind data available for the public. This set the stage for the Danish wind industry's success, with over 4600 of the 11,000 wind turbines installed in the 1980s being of Danish origin. US Windpower was the most successful American wind turbine manufacturer, installing 2700 wind turbines by 1986 (Gipe & Möllerström, 2023).

It has been suggested that Denmark's lack of aerospace industry helped in its supremacy when it came to wind turbine manufacturing. When it came down to it, wind turbines and aircraft were different and benefited from different design philosophies. Besides its efficiency, it is important to minimize a wind turbine's maintenance costs and have it run unattended for as long as possible. This is really not an issue with aircraft. Thus the giant projects attempted by the aerospace companies of other countries, who thought that they had the technology in hand, were not that successful. Instead, the danish building up on their traditional knowledge of wind turbine design, slowly perfected their craft through research and experimentation to reach the level of sophistication that allowed them to build the complicated machines other countries tried to build from their purely aerospace base. As a result, Denmark was able to address 50 % of its electricity needs through wind energy alone in 2020 (Gipe & Möllerström, 2023).

Wind turbines have come a long way during the past century. Modern wind turbines produce 10 times as much power as the earliest wind turbines of the same size. The sizes of modern wind turbines is also much larger than even ones as recent as the 1980s, being more than 100 times in area. The rated power has also been increasing until the mid-2010s when a move to interior less windy locations flattened that trend (Gipe & Möllerström, 2023).

## 2.4. Wind Resource Assessment

Wind resource assessment is key for any wind project, because the power has a cubic relationship with the wind speed. Wind speeds vary with location and time. In the preliminary assessment phase, several activities are used to find out wind data including collecting airport or weather station data and studying area topography, flagged trees, or other indicators. In older times, the wind speed and the prevailing wind direction were estimated by looking at the inclination of some trees. Typically though, further wind measurement data is used to more precisely estimate the wind power potential (WPP) of a site.

On-site wind speed measurement provide a more accurate estimate of WPP than the other indicators mentioned above. Four year measurement are used for short term analysis, and 10 years are recommended for long term analysis. Data is recorded every 1 min, 10 min, or 1 hour. The 10 min time series data is recommended by most of the literature. Instead of handling such huge data, typically, a statistical distribution is used to model the data. Weibull and Rayleigh distributions are the most widely used distributions. These distributions compress the huge data into two and one parameters for Weibull and Rayleigh respectively. The two weibull parameters are $k$, the shape parameter, and $c$, the scale parameter. Rayleigh distribution is a special case of Weibull distribution with $k=2$. The mathematical representation of the Weibull probability distribution for modeling wind speeds and its cumulative probability function are given in equations 2.1 and 2.2 respectively.

$$f(v)=\left(\frac{k}{c}\right)\left(\frac{v}{c}\right)^{k-1}\exp\left[-\left(\frac{v}{c}\right)^{k-1}\right] \tag{2.1}$$

$$F(v)=1-\exp\left[-\left(\frac{v}{c}\right)^{k-1}\right] \tag{2.2}$$

In addition to location, wind speed also varies with height. The velocity dependence on height is captured in the power law shown in equation 2.3 below.

$$\frac{v_2}{v_1}=\left(\frac{h_2}{h_1}\right)^{\alpha} \tag{2.3}$$

Where $v_1$ is the wind speed at the reference height $h_1$, and $v_2$ is the required velocity at the hub height $h_2$. $\alpha$ is the power law exponent taken to be 0.143. A logarithmic law is also shown in equation 2.4 which includes the additional term $z_0$, which is the roughness height measuring the effect of ground topography on the wind speed.

$$\frac{v_2}{v_1}=\frac{\ln(h_2/z_0)}{\ln(h_1/z_0)} \tag{2.4}$$

## 2.5. Types of Wind Turbines

Wind turbines can be classified according to various metrics. One is the type of aerodynamic force the turbine blade uses to operate. Lift-type wind turbines have lifting surfaces and exploit the lift force to generate power. Drag type wind turbines on the other hand use the drag force incident on the rotor. It is important to note that the theoretical maximum efficiency that can be obtained from lift-type wind turbines is almost twice as much as those for drag-type wind turbines (Hau & Hau, 2006). For this reason. Lift-type wind turbines are the most commonly used type of wind turbines.

Wind turbines can also be classified according to the direction of their axis of rotation. Wind turbines with their axes of rotation parallel to the ground are known as horizontal-axis wind turbines and wind turbines with their axes perpendicular to the ground are known as vertical-axis wind turbines. All horizontal-axis wind turbines encountered in practice are lift-type while both lift-type and drag-type vertical-axis wind turbines can be found.

The most common types of vertical-axis wind turbines are the Darrieus, Savonius and H-rotor turbines. The Darrieus turbine was proposed by Darrieus in 1925. It is a lift-type machine that has curved blades, curved in the shape of a troposkein. A troposkein is the shape a rope anchored at both ends takes when rotated in a vertical axis. Since it is the natural shape taken by a flexible element that does not support any bending loads, a rigid object having this shape rotating at just the right speed will also have no bending loads, and will only be loaded in tension. The Darrieus turbine has theoretically the same high efficiencies seen in horizontal-axis wind turbines. A derivative of the Darrieus turbine is the H-rotor turbine. This turbine solves does away with the curved blades and utilizes straight blades for ease of manufacture. However, the production costs of these turbines still cannot compete with horizontal-axis wind turbines (Hau & Hau, 2006).

Another type of vertical-axis wind turbine is the Savonius turbine. This is typically a drag-type wind turbine. It has a low efficiency as a result, but it has a good starting torque. Its rugged construction and high torque make it ideal for simple applications such as pumping water and ventilating railroad carriages and delivery vans (Hau & Hau, 2006). These popular examples of vertical-axis wind turbines are shown below in figure 2.3.

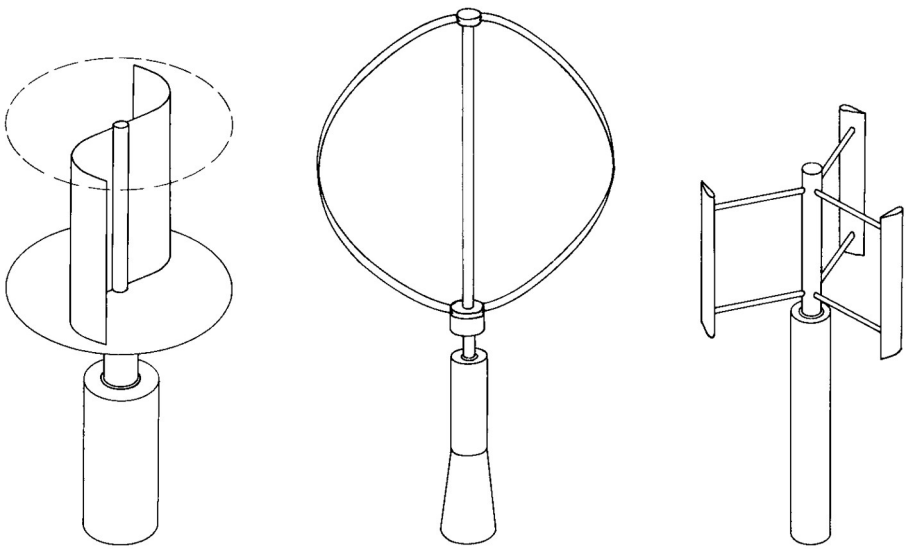

*Figure 2.3: Vertical-axis wind turbine rotor concepts; Savonius rotor (left), Darrieus rotor (center), and H-rotor (right) (Hau & Hau, 2006)*

A general benefit of vertical-axis turbines is that they have the generator and gearbox on the ground where it is easier to maintain. Additionally, they can operate under winds coming from any direction and thus do not need a yaw system. Their disadvantages include, low rotational speed (which negatively affects the efficiency of the machine), inability to self-start, and inability to control the power output of the turbine by pitching the blades (Hau & Hau, 2006).

Horizontal-axis wind turbines have seen much success in the market due to a few reasons. The fact that the power output can be controlled by pitching the blades is important as it allows for good low speed performance as well as protects the turbine by decreasing lift at high wind speeds. Additionally, horizontal-axis wind turbines are very similar to propellers and benefit from the prior body of knowledge accumulated from work on propellers (Hau & Hau, 2006).

Other concepts also exist comprising new ways of harnessing wind energy or augmenting the efficiencies of the concepts mentioned above. Most attempts at increasing the efficiencies of turbines past the theoretical maximum of the previous concepts revolve around providing some kind of enclosure around the turbine. A ducted rotor places a constant diameter duct around the turbine which prevents the flow from narrowing during intake allowing a theoretical maximum $c_p$ of 0.66. Using a diffuser behind the turbine has also been proposed, which can raise the $c_p$ to 0.75 even when the reference area of the maximum diameter of the diffuser is used. Another concentrator technology is the vortex tower which uses the low pressure from a vortex generated by a vertical cylinder with vertical vents to draw air through a turbine. Experiments show, however, that it has a low $c_p$ of 0.1 (Hau & Hau, 2006).

Another approach uses stator blades to create a swirl in the incoming wind impacting a horizontal-axis wind turbine. While an increase in efficiency is seen, the strength of the stator during high-speed winds is of particular concern. Yet another concept uses temperature gradient created by heating air in a canopy using solar energy to drive the air up a chimney which houses a turbine. This concept becomes more efficient when the area covered by the canopy is high (Hau & Hau, 2006).

Another concept, called a bladeless turbine, uses vortex induced oscillations to produce electricity. This is still a very new concept, however, and needs more research to ascertain its viability (Tandel et al., 2021). An electrostatic wind energy convertor operates by using the wind to transport charged particles against an electric field to generate electricity. It is also a new concept, and the conversion efficiency is still very low (Djairam et al., 2005). Some of these novel concepts are shown in figure 2.4.

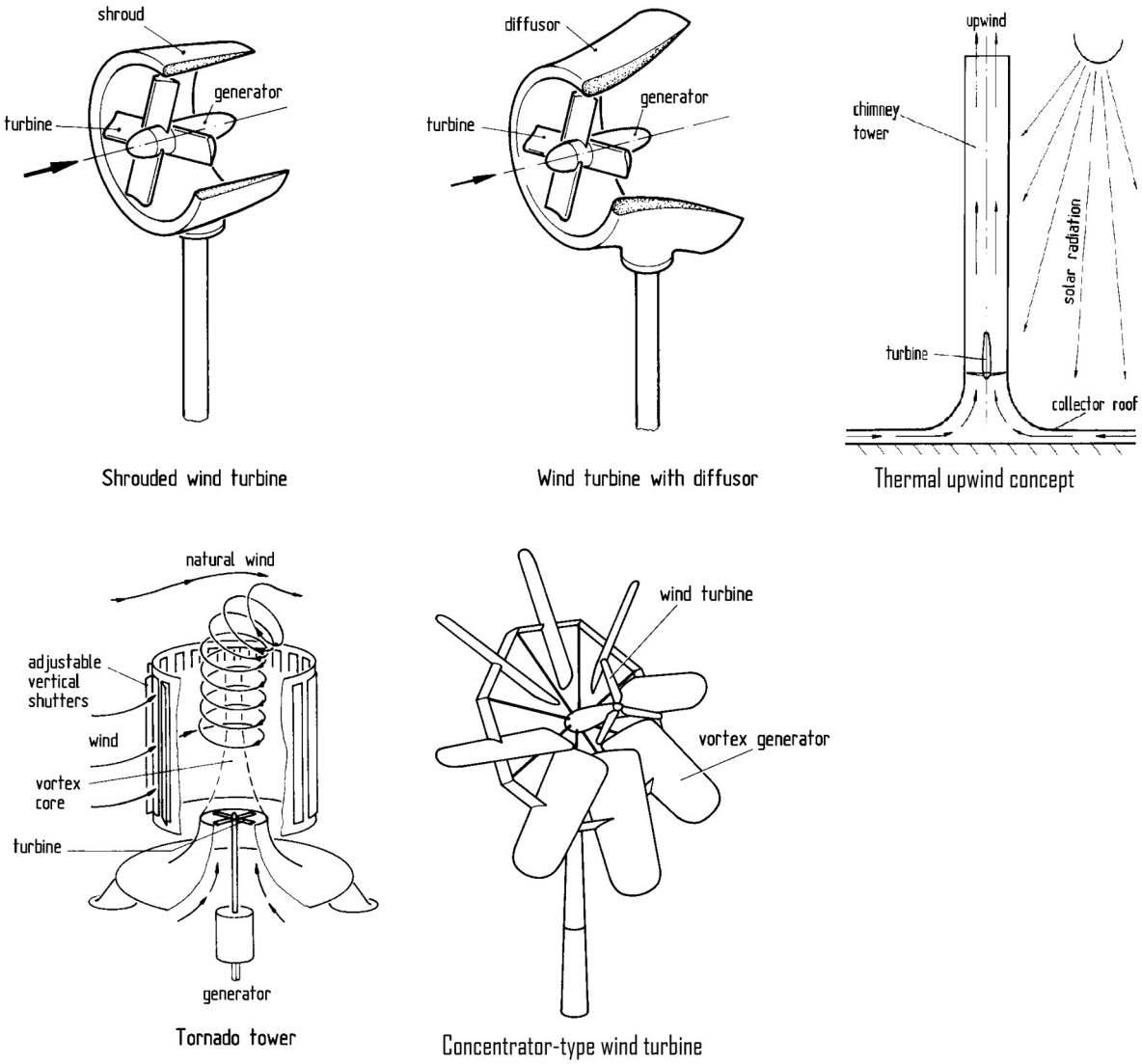


*Figure 2.4: Various alternative wind turbine concepts (Hau & Hau, 2006)*

Wind turbines can also be classified as based on their size. The IEC safety standards for small wind turbines, IEC 61400-2 defines small wind turbines to be those that have less than 200 $m^2$ of swept area which corresponds to a power of less than 50 kW. While the exact demarcation line is less important, it is important to understand the different issues that arise with the variation of scale. Small wind turbines have to be located close to the point of use since it is not economical to incur the cost of transmission of the small amount of energy they provide. Thus, they are likely to be located in less windy sites than their larger counterparts. Additionally, the generators used for small wind turbines have high resisitive torques at start up. As a result their optimizing their low speed and starting performance is key to their overall performance. Additionally, the Reynolds numbers encountered are different because of the variation in the dimensions of the blades. This also must be considered in their aerodynamic analysis (Wood, 2011).

## 2.6. Components of Small Horizontal Axis Wind Turbines

The following components or systems are found in horizontal axis wind turbines.

### 2.6.1. Blade

The blade of the turbine is the component that converts the axial motion of the wind into a rotary motion. As HAWTs are lift type machines, the sections of the blades are airfoils which generate as much lift as possible while limiting drag. The line connecting the front and rear ends of the airfoil is called the chord line. The length of this chord can be varied across the longitudinal direction, also known as span, of the blade. The angle between the rotation plane and the chord line is known as the twist, $\theta_p$. The twist is also typically varied across the span of the blade to achieve a good performance. In large wind turbines, the whole blade can be pitched in the longitudinal axis, effectively adding the pitch angle to the twist at each section. The blades of large wind turbines are mostly made of fiberglass. Small wind turbines have been known to be made with composite materials or wood. A diagram of a typical wind turbine blade is shown below in figure 2.5.

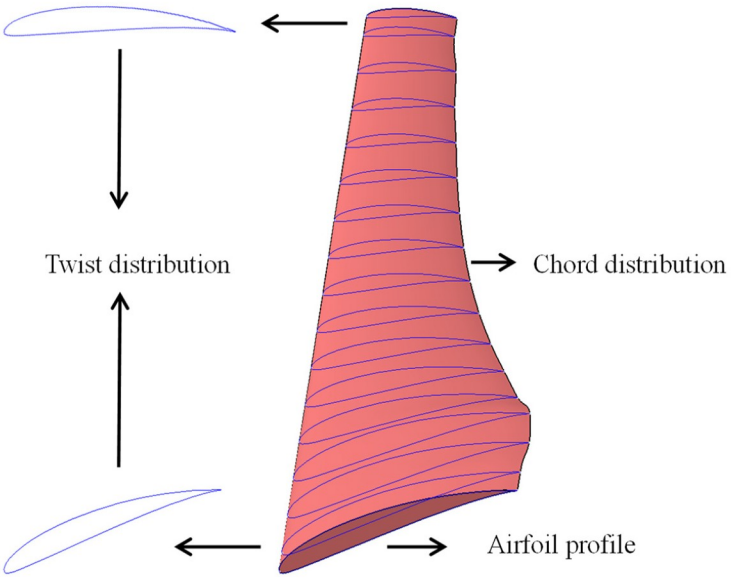


*Figure 2.5: Twist and chord distribution of a blade (Akbari et al., 2022)*

### 2.6.2. Generator

The generator converts the rotary motion of the rotor into electricity. There are generally four types of generator systems used in wind turbines (Polinder et al., 2013).

The first type is the constant speed squirrel-cage induction generator. It contains a three stage gearbox and a squirrel-cage induction generator and is capable of producing up to 1.5 MW of power. The generator is efficient at the rated wind speed. When the wind speed is above the rated wind speed, the blades stall decreasing the lift and hence preventing the power from increasing

further. Usually, the blades are designed to stall at high speeds, but sometimes active stall by pitching the blades is used. This system can be built from simple components and is thus cheap. However, its efficiency suffers as it peaks around a single rated speed. Some variations exist to mitigate this drawback and allow efficient operation over a wider speed range (Polinder et al., 2013).

The next type of generator system is the doubly fed induction generator. These came later than constant speed squirrel-cage induction generators and could work efficiently at a wider range of wind speeds. This system also provided greater flexibility in catering to noise, load, energy yield, and power quality. This system could not stay connected under short periods of low voltage, also known as grid fault ride-through capability, but this problem has since been solved (Polinder et al., 2013).

Then came brushless generators which were developed to address the grid fault ride-through issue of DFIGs. They also have lower maintenance requirements because they are brushless. Direct drive generators also exist. These use a synchronous machine and they don't have gearboxes. Electrical excitation as well as permanent magnets have been used to create a magnetic field. These generators are larger, heavier, and more expensive than high-speed generators that use a gearbox. However, the lack of gearbox has been cited as a reason for increasing the reliability of the system (Polinder et al., 2013).

Most of the machines above are mainly used in large wind turbines. For small wind turbines, permanent magnet direct drive generators are economical. These are efficient at low speeds, have no gearboxes, and are easy to control. However, the magnet loses some of its magnetism over time. Some also use induction generators due to their low cost and robustness. But these get less efficient at small sizes and small loads. They also need excitation which might not work in some cases like when a sudden increase in wind speed occurs when the blades are at rest (Wood, 2011).

### 2.6.3. Tower

The tower provides structural support for the blades and generator. Four types of towers are encountered in practice for small wind turbines. Monopole towers are comprised of a single pole and are made by bending sheets of steel and seam welding them. The optimal shape is circular, but octagonal sections are frequently encountered because of their ease in manufacturing. They are made in multiple sections and joined by slip-fitting followed by bolting or by bolting using flanges. They are more aesthetically pleasing than the rest, however they require more material and hence are expensive to manufacture and transport (Wood, 2011).

Guyed towers use cables to support a central pole. They require less material and hence are cheaper than monopoles. Additionally, the natural frequency of the tower can be adjusted by adjusting the tension in the guy wires. The wires also provide good grounding for lightning. However, they cannot be used in urban areas since they require more area and can be easily vandalized (Wood, 2011).

*Figure 2.6: Different types of towers: Monopole tower (left), lattice tower (top right), and guyed tower (bottom right) (Westwood, 2012; Wood, 2011)*

The other type of tower is the lattice tower. It can be a sectional lattice or tubular lattice tower. Sectional lattice towers are made from angle or other steel sections and are assembled on site. They are also cheap to transport. However, they have a shorter life than other tower types because they are liable to corrosion at their joints. Tubular towers are prefabricated in sections before they arrive on site. They are easy to manufacture and are light and stiff. They also last long even without galvanizing. However, they provide little protection for electrical cables (Wood, 2011). The various kinds of towers encountered in practice for small wind turbines are shown in figure 2.6.

### 2.6.4. Speed Control System

Since wind is inherently a highly random energy source, wind turbine control plays a very important role. It works to maximize power production, decrease loads, and ensure a continuous power production. It achieves this by controlling the blade pitch or/and the generator torque of the turbine. The coefficient of power, $C_p$, is optimal at some pitch angle and tip speed ratio. The blade tip speed ratio, which is the ratio of the blade tip speed and the wind speed, can then be controlled by varying the generator torque to follow a Maximum Power Point Tracking (MPPT) strategy. The control system also controls the electrical power that is delivered to the grid or other consumer (Novaes Menezes et al., 2018).

Generally, there are four regions of operations in which the control system has different objectives. Below the cut-in speed, which is the speed below which the wind is not strong enough to move the turbine blades, the turbine is made out of operation. Between the cut-in speed and the rated speed, the control system tries to maximize power production. The rated speed might be achieved, but the torque may still be below the rated torque. In such cases, the speed is kept constant, while the torque is allowed to vary up to its rated value. When the rated power is reached, the control system tries to keep the power produced at the rated power by using pitch control. When the wind speed is above the cut-out wind speed, in which it is unsafe for the turbine to operate, the wind turbine is stopped (Novaes Menezes et al., 2018).

In small wind turbines, the rotor is usually faced out of the wind when the wind speed exceeds the cut-out speed. This strategy is known as furling. It occurs when the tail collapses around the furling axis. Normally it is held in place by its own weight which is overcome during high winds by the aerodynamic moment on the fin. Since the rotor axis is offset from the yaw axis, the rotor thrust then pushes the turbine out of the wind. Large wind turbines, on the other hand, have brakes which are activated when the wind speed is excessive.

In wind turbines that use squirrel cage induction motors with no power converters, torque control is not possible and the generator speed is tied to the frequency of the grid. More modern generators like DFIG and DD generators employ a two-layer cascaded controller. The outer loop decides the operating torque via an MPPT strategy, while the inner loop adjusts the frequency using an electronic power converter (Novaes Menezes et al., 2018).

While pitch control is common in large turbines, early wind turbines and modern small wind turbines employ stall regulation to reduce the power output. The blades of these turbines are

designed to generate less lift above the rated speed. This is a very cost effective control means, but it is subject to power fluctuations, torque spikes and varying loads (Novaes Menezes et al., 2018).

### 2.6.5. Yaw Control System

Horizontal-axis wind turbines need to face the wind to produce power. If there is a yaw error of $\theta$, the power is reduced by a factor of $\cos^2(\theta)$. This can be done actively by using a motor or passively by using a tail fin. Most small wind turbines use a tail fin. A small yaw error is always present when tail fins are used because the rotor axis is offset from the yaw axis and the thrust of the rotor produces a moment that counteracts the tail fin moment. Gyroscopic load on the blades can be significant when yawing and must be considered when designing the tail fin (Wood, 2011).

In actively controlled yaw systems, the need for immediate yawing is counterbalanced by consideration for the long life of the system. Thus, yawing delays are implemented which are inversely proportional to the amount of yaw that is needed (Hau & Hau, 2006).

## 2.7. Design of Small Wind Turbine Blades

### 2.7.1. Important Parameters

The power output as well as the torque are known to be correlated to the air density $\rho$, the viscosity $\nu$, the wind speed $U_0$, the blade radius $R$, and the rotor speed Ω. Dimensional analysis of these relations yields several important parameters in the design of wind turbines. The first of these is the coefficient of power, $C_p$. This dimensionless parameter expresses the fraction of kinetic energy present in the wind that has been harnessed. Its formula is shown in equation 2.5. As will be discussed next, this value has a maximum, dictated by the Betz limit, for unshrouded wind turbines.

$$C_p = \frac{P}{\frac{1}{2}\rho U_0^3 \pi R^2} \tag{2.5}$$

The other important parameter is known as the tip-speed ratio, $\lambda$. This is the ratio of the blade tip to the wind speed. This relation is shown in equation 2.6. A local tip-speed ratio, $\lambda_r = \lambda r/R$ can also be defined. The tip-speed ratio is affects the angle of attack at the blade sections. When operating at maximum $C_p$, the tip-speed ratio ranges from 7-10 for most wind turbines. Those that are used to pump water typically operate at lower tip-speed ratios.

$$\lambda = \Omega R / U_0 \tag{2.6}$$

Another parameter obtained from dimensional analysis is the Reynolds number. This is important because it affects the lift and drag that is encountered. It depends on the total wind speed at the

blade, $U_{res}$, the chord length, c, and the kinematic viscosity of air, $\nu$. This relation is shown in equation 2.7. Small wind turbine operate at lower Reynolds numbers than large wind turbines and airplanes, typically less than 500,000. Thus, it can be difficult to get accurate lift and drag experimental data since the data that is usually found caters to these high Reynolds number applications (Wood, 2011).

$$Re = U_{res}\, c/\nu \tag{2.7}$$

Similar to the power coefficient, a thrust coefficient can be defined as in equation 2.8. This serves as a non-dimensional thrust force.

$$C_T = \frac{T}{\frac{1}{2}\rho U_0^2 \pi R^2} \tag{2.8}$$

The annual energy performance (AEP) is another parameter that we are interested in. The coefficient of power gives the performance of the turbine at some wind speed. The AEP, on the other hand, allows us to take into consideration the variation of wind speed. It is simply the amount of energy harnessed by the turbine over a period of a year. It can be obtained by summing the energy contributions of a range wind speeds between the cut-in wind speed, $V_{ci}$, and the cut-out wind speed, $V_{co}$. Each contribution is multiplied by the probability of occurrence P(V) of wind speeds within $\Delta V/2$ of the wind speed V. This relation is shown in equation 2.9.

$$AEP = 8760 \sum_{V_{ci}}^{V_{co}} \frac{1}{2} C_p \rho V^3 \pi R^2 P(V) \Delta V \tag{2.9}$$

Finally, the cost of energy is the cost of producing a unit of energy. It is very useful because it is the metric that determines if the wind turbine is economically useful or not. It is calculated by dividing the annual cost of the turbine with the annual energy production. There are up front costs which include the turbine capital cost and the balance of system costs (various upfront costs such as site development, management, site preparation, foundation construction, turbine erection, collection system construction, grid connection and substation construction). Then there are ongoing costs which include operation and maintenance costs. The upfront costs are multiplied by a fixed charge rate to take into account the higher value of earlier costs and to convert the cost into an annual cost. This fixed charge rate depends on the market, but is assumed to be 6.73% (Stehly et al., 2023). The total relation is shown in equation 2.10.

$$COE = \frac{FCR \times (TC + BOS) + OM}{AEP} \tag{2.10}$$

Where

*TC* is the turbine cost,

*FCR* is the fixed charge rate,

*BOS* is the balance of system costs, and

*OM* is the operation and maintenance costs.

### 2.7.2. Momentum Theory and the Betz Limit

Momentum theory is a theory based on control volume analysis and conservation that gives us a simple relation between the turbine's operating parameters. It assumes the presence of an imaginary actuator disc where the turbine rotor is located which extracts energy out of the air, as seen in figure 2.7. As the air passes through the disc it abruptly loses pressure while the velocity remains continuous.

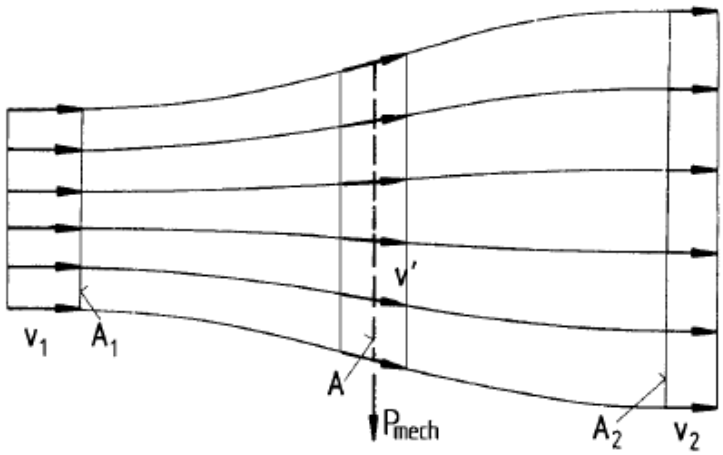


*Figure 2.7: Idealized flow through an actuator disc according to momentum theory (Hau & Hau, 2006)*

Assuming the flow is incompressible, it is easy to find that the maximum $C_p$ of $16/27 \approx 0.593$ occurs at $a = 1/3$, where $v = (1-a)v_1$ and $v_2 = (1-2a)v_1$. This is known as the Betz limit which specifies a maximum coefficient of performance for unshrouded wind turbines. The coefficient of power for large wind turbines is currently around 0.5 (Wood, 2011). This is because of the assumptions that were made in the derivation including the assumption that the flow is inviscid, that the flow is uniform and the absence of radial flow. Some of these assumptions like uniform flow will be corrected for in blade element momentum theory.

### 2.7.3. Aerodynamics of Wind Turbine Blades

As mentioned before, the sections of wind turbine blades are airfoils. An airfoil is a two-dimensional shape that can generate lift while keeping drag to a minimum. The lift force, L, is

generated perpendicular to the direction of airflow while the drag force, D, is generated in the direction of the air flow.

The National Advisory Committee on Aeronautics (NACA), which was the precursor of NASA, developed its four digit NACA series in the 1920s. The first digit of the four digit NACA series represents the amount of camber in percentage of the chord. The camber is the maximum distance between the mean camber line, which is the line whose points lie halfway between the upper and lower surfaces, and the chord line. The chord line is a straight line that joins the leading edge and trailing edge of the airfoil. A camber of 6 % is the maximum for most practical airfoils. The second digit represents the position of the maximum camber in tenths of chord, while the last two digits represent the maximum thickness of the airfoil in percentage of the chord. The position of maximum thickness is 40 % for all four digit NACA airfoils. Using these facts, one can specify equations for the airfoil surfaces as these airfoils could be analytically described. Modern airfoils in general, however, need the specification of the coordinates of tens or hundreds of points on their surface to be accurately described.

Airfoils designed specifically for small wind turbines exist. The low Reynolds number experienced by the blades across the entire span necessitate the use of specially designed airfoils. One example is the SG604x family of airfoils (Gigue`re & Selig, 1998).

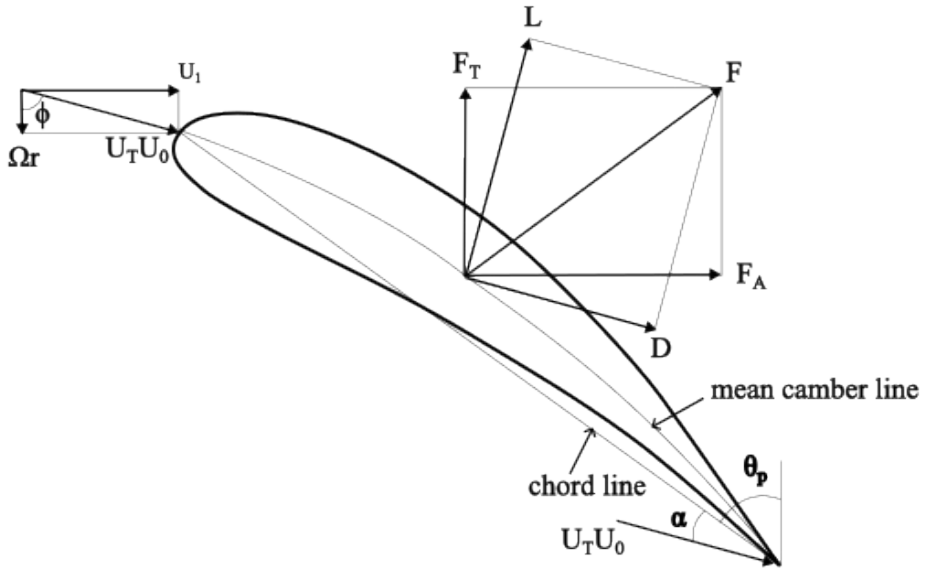


*Figure 2.8: Lift, drag, and relative wind speed at a blade section*

As can be seen in figure 2.8, the relative wind speed, $U_T U_0$, at the blade section has two components. The axial component, $U_1$, which is due to the wind itself, and the tangential component, $\Omega r$, which is the velocity due to the rotation of the blades. $U_T$ is the non-dimensional

velocity at the blade normalized by the free-stream wind speed $U_0$. The inflow angle, $\phi$, is the angle between the plane of rotation of the blade and the resultant relative velocity. The angle between the plane of rotation and the chord line is called the pitch angle, $\theta_p$. The angle between the chord line and the relative wind velocity is called the angle of attack, $\alpha$. The relation shown in equation 2.11 between these angles can be seen from figure 2.8.

$$\theta_p + \alpha = \phi \tag{2.11}$$

The lift and drag forces per length can be found from the formulas in equations 2.12 and 2.13.

$$L' = \frac{1}{2} C_l \rho c U_T^2 U_0^2 \tag{2.12}$$

$$D' = \frac{1}{2} C_d \rho c U_T^2 U_0^2 \tag{2.13}$$

$C_l$ and $C_d$ are the lift and drag coefficients which depend on the shape of the airfoil, the angle of attack, and the Reynolds number. They can be obtained experimentally or numerically. It must be stressed that the airfoil is two-dimensional while a turbine blade is a three-dimensional object. The lift and drag of the actual turbine blade is a little different from integrating the airfoil lift and drag per length across the span. The parameter that is responsible for this difference is the Aspect Ratio, *AR*. It is the ratio of the span $b$ and average chord $c$ of the blade. As the aspect ratio approaches infinity, the actual lift and drag coefficients approach that of their two dimensional approximations. The aspect ratio for most wind turbine blades is large (10 – 30) which makes the impact of *AR* small at low angles of incidence. At high angles of incidence however, *AR* effects can be significant (Wood, 2011).

The lift and drag coefficients are a function of both angle of attack and Reynolds number. Typically, the lift increases linearly up to some angle of attack called the stall angle. Then there is a sudden loss of lift due to separation of the flow on the upper surface. This is known as stalling. The drag usually stays constant before stall and increases rapidly after stalling. Therefore the angle giving the maximum lift-to-drag ratio, which represents a point close to the efficient angle of attack, lies just before stall. This angle of maximum lift-to-drag ratio depends on the Reynolds number. Thus a wind turbine with no pitch control cannot continually operate at this point when the wind speed varies (Wood, 2011).

The twist at the tip is close to 0° because the tangential velocity is much greater than the axial velocity. As a result, when the blades are at rest, angles of attack close to 90° can be seen. Thus, the starting performance of the turbine depends on the performance of the airfoils at these high angles

of attack. Typically, the airfoil can be approximated as a flat plate at these high angles of attack. The lift and drag coefficients can also be calculated as in equations 2.14 and 2.15.

$$C_l = A \sin 2\alpha \tag{2.14}$$

$$C_d = B - C \cos 2\alpha \tag{2.15}$$

$A$, $B$, and $C$ are airfoil and Re dependent, especially at low Reynolds numbers (Wood, 2011).

The lift and drag can be decomposed in to axial and tangential components as in equations 2.16 and 2.17 to compute the thrust and torque per length, $dT$ and $dQ$ respectively of all $N$ blades.

$$dT = N\left[L' \cos(\phi) + D' \sin(\phi)\right] dr = \frac{1}{2} N \rho c U_T^2 U_0^2 \left(C_l \cos(\phi) + C_d \sin(\phi)\right) dr \tag{2.16}$$

$$dQ = \left[L' \sin(\phi) - D' \cos(\phi)\right] r\, dr = \frac{1}{2} N \rho c U_T^2 U_0^2 \left(C_l \sin(\phi) - C_d \cos(\phi)\right) r\, dr \tag{2.17}$$

When integrated across the span, these parameters give the thrust, $T$, and the torque, $Q$ on the blades.

The Kutta-Joukowsky theorem relates the lift produced by an airfoil to the circulation around it. This relation is shown in equation 2.18. The circulation, $\Gamma$, is the line integral of the velocity tangent to any path encircling the airfoil, mathematically defined in equation 2.19.

$$L' = \rho V \Gamma \tag{2.18}$$

$$\Gamma = \oint \vec{U} \cdot \vec{dl} \tag{2.19}$$

Where $\vec{U}$ is the air velocity and $\vec{dl}$ is the differential increment along the path. Similar to aircraft wings, an optimum chord distribution, shown in equation 2.20, can be calculated by analyzing the circulation. It turns out that a constant circulation along the span yields performance that is close to the Betz-Joukowsky limit (Wood, 2011).

$$c = \frac{16\pi}{9 N \lambda C_l \sqrt{4/9 + \left[\lambda_r + 2/(9\lambda_r)\right]^2}} \tag{2.20}$$

### 2.7.4. Blade Element Momentum Calculations

Blade Element Theory divides the blade into finite blade elements which have constant parameters across their spans. Radial velocity of the air is ignored. Combining it with momentum theory with its actuator disk gives Blade Element Momentum Theory. Instead of applying conservation equations on a control volume containing the entire disc, we apply conservation equations on annular streamtubes, each streamtube being identified with a blade element. This streamtube is shown in figure 2.9.

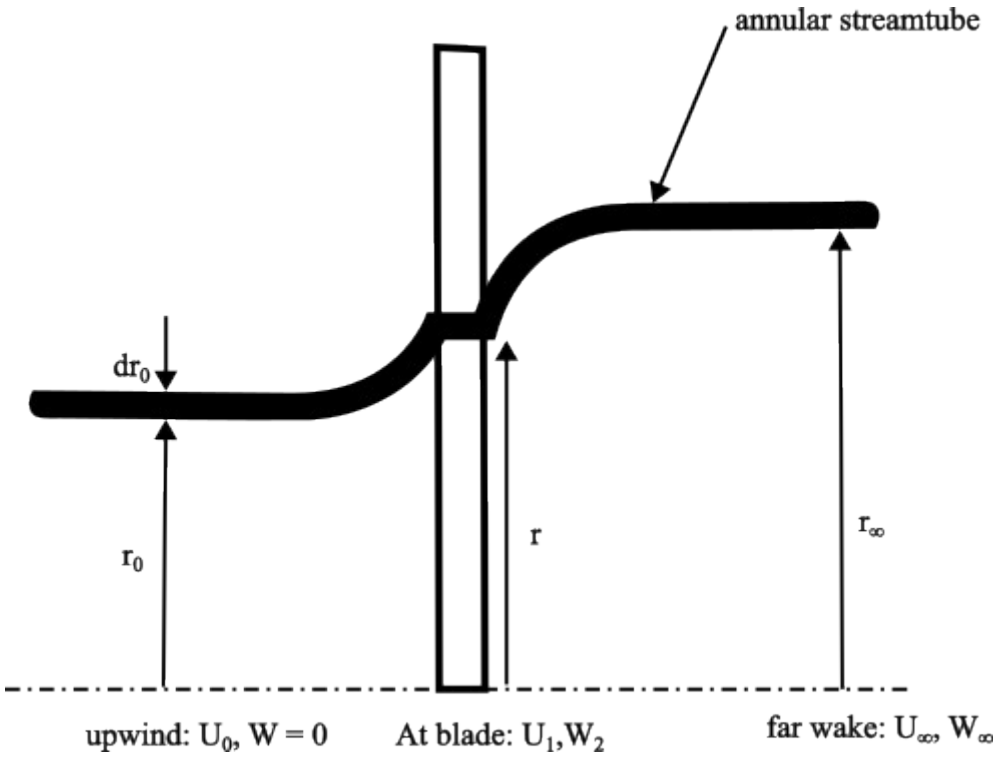


*Figure 2.9: Annular streamtube (Wood, 2011)*

Applying the conservation of mass at the three positions, we arrive at equation 2.21.

$$U_0 2\pi r_0 dr_0 = U_1 2\pi r\, dr = U_\infty 2\pi r_\infty dr_\infty \tag{2.21}$$

From which we can derive equation 2.22.

$$U_0 r_0 dr_0 = U_1 r\, dr = U_\infty r_\infty dr_\infty \tag{2.22}$$

Conservation of linear momentum can also be applied by specifying the momentum flowing in and out of the streamtube to get the thrust on the control volume as seen in equation 2.23.

$$dT = \rho U_0 U_0 2\pi r_0 dr_0 - \rho U_\infty U_\infty 2\pi r_\infty dr_\infty = 2\pi\, \rho U_1 r (U_0 - U_\infty) dr \tag{2.23}$$

Defining the axial inflow factor $a$ as before, we have equations 2.24 and 2.25. Using these we can modify equation 2.23 into equation 2.26.

$$a = 1 - U_1/U_0 \tag{2.24}$$

$$U_\infty = (1-2a)U_0 \tag{2.25}$$

$$dT = 4\pi\rho U_0^2 r\, a(1-a)\, dr \tag{2.26}$$

Similarly, applying the conservation of angular momentum, we have the expression for the torque in equation 2.27.

$$dQ = \rho r_\infty W_\infty U_\infty 2\pi r_\infty dr_\infty = 2\pi\rho U_0(1-a)W_2 r^2 dr = 4\pi\rho U_0(1-a)a'\Omega r^3 dr \tag{2.27}$$

Since the angular momentum is conserved downstream of the turbine, the fact that $r W_2 = r_\infty W_\infty$ was used in the previous equation. Additionally, a rotational interference factor $a'$ is defined where $W_2 = 2a'\Omega r$. $a'$ can be understood as the non-dimensional increase of the tangential velocity between the upstream flow and the middle of the blade or the middle of the blade and the far wake. It is assumed that the tangential velocity develops over the blade and the average tangential speed is given in equation 2.28.

$$W = (W_0 + W_2)/2 = W_2/2 = a'\Omega r \tag{2.28}$$

The resultant non-dimensional wind velocity relative to the blade elements can be expressed as a function of the tangential and axial induction factors as seen in equation 2.29.

$$U_T^2 = (1-a)^2 + [(1+a')\lambda_r]^2 \tag{2.29}$$

Combining the two expressions for $dT$, equation 2.16 and equation 2.26, we have equation 2.30.

$$4\pi\rho U_0^2 r\, a(1-a)\, dr = \frac{1}{2} N \rho c\, U_T^2 U_0^2 (C_l \cos(\phi) + C_d \sin(\phi))\, dr \tag{2.30}$$

Similarly, combining the two expressions for $dQ$, equation 2.17 and 2.27, we have equation 2.31.

$$4\pi\rho U_0(1-a)a'\Omega r^3 dr = \frac{1}{2} N \rho c\, U_T^2 U_0^2 (C_l \sin(\phi) - C_d \cos(\phi)) r\, dr \tag{2.31}$$

Simplifying equation 2.30 and 2.31, we get equations 2.32 and 2.33.

$$a(1-a) = \frac{\sigma U_T^2 C_a}{4} \tag{2.32}$$

$$(1-a)a'\lambda_r = \frac{\sigma U_T^2 C_{a'}}{4} \tag{2.33}$$

Where $\sigma$ is the solidity of the turbine given by $\sigma = Nc/2\pi r$, $C_a = C_l\cos(\phi) + C_d\sin(\phi)$, and $C_{a'} = C_l\sin(\phi) - C_d\cos(\phi)$.

Equation 2.34 shows the relationship between the inflow angle $\phi$ and the interference factors.

$$\tan\phi = \frac{1-a}{\lambda_r(1+a')} \tag{2.34}$$

Eqs. 2.32 and 2.33 form a system of non-linear equations in the form of equations 2.35 and 2.36 that can be solved through iteration.

$$a_{n+1}(1-a_{n+1})=f_a(a_n,a'_n) \tag{2.35}$$

$$a'_{n+1}=a_{n+1}f_{a'}(a_n,a'_n) \tag{2.36}$$

Where $f_a=\frac{\sigma U_T^2 C_a}{4}$ and $f_{a'}=C_{a'}/(C_a\lambda_r)$.

One assumption we have been making so far is that the flow is uniform tangentially across the annulus. In reality, however, the flow close to the blades and away from the blades is different. This presents a problem because equations 2.26 and 2.27 were derived for the entire annulus using average velocities while equations 2.16 and 2.17 were derived using velocities close to the blade. There needs to be a parameter that links the average velocities to velocities near the blade. This parameter is known as Prandtl's tip loss factor, $F$. $F=a/a_b$ where $a_b$ is the axial induction factor at the blades and $a$ is the average axial induction factor. The tip loss factor can be calculated as in equation 2.37.

$$F=2\cos^{-1}\left(e^{-(N(R-r)/(2r\sin\phi))}\right)/\pi \tag{2.37}$$

This value can make up to 5 – 10 % difference in the predicted turbine performance.

Thus equations 2.32 and 2.33 can be rewritten as equations 2.38 and 2.39.

$$\frac{a_b F(1-a_b F)}{(1-a_b)^2}=\frac{\sigma C_a}{4\sin^2\phi} \tag{2.38}$$

$$\frac{a'_b F(1-a_b F)}{(1+a'_b)(1-a_b)}=\frac{\sigma C_{a'}}{4\sin\phi\cos\phi} \tag{2.39}$$

And equation 2.34 can be rewritten as equation 2.40.

$$\tan\phi=\frac{1-a_b}{\lambda_r(1+a'_b)} \tag{2.40}$$

Another issue to take into account is the fact that momentum theory is not valid for high values of the axial induction factor. According to momentum theory, the thrust coefficient is zero when $a$ is 1. This is physically not realistic since the turbine will instead experience high thrust when it starts to enter into what is called the propeller brake region. Instead, a different relation is used for high values of $a$. This relation is shown in equation 2.41 (Clifton-Smith, 2009).

$$f_a=\begin{cases} a_b F(1-a_b F) & a_b\le a_c \\ a_c^2F^2+(1-2a_c F)a_b F & a_b>a_c \end{cases} \tag{2.41}$$

Where the cut-off value $a_c$ is 1/3. Then equation 2.38 can be generalized into equation 2.42.

$$\frac{f_a}{(1-a_b)^2}=\frac{\sigma C_a}{4\sin^2\phi} \tag{2.42}$$

### 2.7.5. Structural Analysis of Wind Turbines

The IEC 61400-2 is a safety standard for small wind turbines that details the structural analysis requirements in their design. The standard allows analysis using three methods: the Simple Load Model, aero-elastic modeling, and load measurements. The Simple Load Model (SLM) describes a series of simple equations. Due to the rough nature of these equations, the safety factors used are high. Aero-elastic modeling consists of a more detailed computer modeling, which include responses to stochastic inputs such as gusts and wind direction changes. This approach is usually reserved for large wind turbines due to its high cost and lengthy time requirement. Load measurements require field testing with extrapolations for extreme conditions.

The simple load model can only be applied to horizontal axis wind turbines with two or more rigid blades. The first step in the simple load model is to identify which class the turbine belongs to based on the average and reference wind speeds. The different wind turbine classes are shown in table 2.2. Afterwards parameters such as design rotational speed, design wind speed, design shaft torque, maximum yaw rate and maximum rotational speed are obtained. Following that, the loads for the load cases are calculated and converted to equivalent stresses using appropriate safety factors. The different load cases investigated in this model are shown in Table 2.3.

*Table 2.2: IEC turbine classes (Wind Turbines. Part 2, Small Wind Turbines, 2013)*

| Class | I | II | III | IV |
|---|---|---|---|---|
| $U_{ref}$ (m/s) | 50 | 42.5 | 37.5 | 30 |
| $U_{ave}$ (m/s) | 10 | 8.5 | 7.5 | 6 |

*Table 2.3: design load cases of the simple load model (Wind Turbines. Part 2, Small Wind Turbines, 2013)*

| Design situation | Load case | Description | Analysis type |
|---|---|---|---|
| Power production | A | Normal operation | Fatigue |
| | B | Yawing | Ultimate |
| | C | Yaw error | Ultimate |
| | D | Maximum thrust | Ultimate |
| Power production plus occurrence of fault | E | Maximum rotational speed | Ultimate |
| | F | Short at load connection | Ultimate |
| Shutdown | G | Shutdown (braking) | Ultimate |
| Parked (idling) | H | Parked wind loading | Ultimate |
| Parked at fault conditions | I | Parked wind loading (maximum exposure) | Ultimate |
| Transport, assembly, maintenance and repair | J | Provided by the manufacturer | Ultimate |

## 2.8. Manufacturing of Small Wind Turbine Blades

### 2.8.1. Conventional Manufacturing

Small blades can be made from timber. The cost of laminating timber is high, so it is practical to machine blades from blanks. As the size of the blades increases, it becomes increasingly difficult to find blanks without knots or other defects. Timber blades can be CNC milled, however this approach is too expensive for high volume production. Copying routers that copy the profile of the blade from a CNC cut master blade are a promising technology to reduce costs (Wood, 2011).

Larger blades are made from composite materials, fiberglass being the usual choice. The blades suffer from conflicting design objectives, a high stiffness to avoid bending beyond the limit and a low inertia to minimize manufacturing and transportation costs in larger blades and to improve starting performance in small blades. Composite blades have almost all their material in a thin laminate on the surface. These laminates contain fibers laid in a resin matrix. The fibers are laid in the radial direction to counteract centrifugal forces and at 45° to the radial direction for torsional stiffness. Several layers of laminates of different orientations can be used. The number and orientation of laminates can also be varied by location (Wood, 2011).

All composite manufacturing methods utilize molds. For large turbines, the molds can be made by machining thin templates, spacing them out across the span and filling the gap with resin and reinforcement. For small turbines, accuracy is more important, so the molds are usually machined (Wood, 2011).

There are many methods for manufacturing composite parts. The most common methods used for composite blade production are Resin Transfer Molding (RTM) and its derivative, Vacuum Assisted Resin Transfer Molding (VARTM). In VARTM, the fiber is placed on a mold which is first covered by a release agent. Then the fiber is covered by a release ply, a resin runner and a vacuum bag. The release ply facilitates the removal of layers above the blade. The resin runner promotes the flow of resin during infusion. A vacuum pump sucks air out of the vacuum bag. At other ports, resin containers are connected through tubes. The vacuum pulls the resin into the vacuum bag. Additionally, it presses the fiber to the mold. Once all the blade area is wetted by the resin, the inlet and outlet tubes are pinched off and the blade is left to cure. Curing is a chemical process where the liquid resin solidifies. Once curing is finished, the layers are removed and the upper and lower halves of the blade, which are produced separately, are trimmed and joined. Joining can be tricky at the leading edge since the surfaces meet in parallel, providing little area for gluing (Wood, 2011). A blade being manufactured by the VARTM process is shown in figure 2.10.

*Figure 2.10: VARTM process (Wood, 2011)*

RTM is similar, with a few key differences. Two mold faces are used for RTM, above and below. Unlike VARTM, the resin is pressure fed into the mold. The temperature is controlled during resin infusion and curing. RTM is more expensive than VARTM, but it can handle complex shapes and provides a good finish on both sides (Mazumdar, 2002).

### 2.8.2. Additive Manufacturing

During the early years of additive manufacturing (AM), the process was used for Rapid Prototyping and Testing. More recently, however, it has been used for large-scale manufacturing. Traditional manufacturing techniques still give better results at very high volumes, but AM processes perform better even when the production volume is in the thousands (Costabile et al., 2017). The cost curve for AM is flat and thus does not benefit from economies of scale (Busachi et al., 2017). Not only does the cost per part stay constant with volume, but it also stays constant with the complexity of the part. This makes AM suitable for parts with features that are difficult to produce with traditional manufacturing techniques like machining or injection molding.

Some work has already been done utilizing 3d printing to produce wind turbine components and manufacturing equipment. In a partnership between Oak Ridge National Laboratory (ORNL) and a small business, XZERES wind, the additive manufacturing of small wind turbine blades was performed. The project aimed at producing 3D printed blades 3 – 5 m in size. As shown in figure 2.11, they 3D printed a modified design of an existing blade using a Big Area Additive Manufacturing (BAAM) system. The printer system was able to print 4 blade sections in 9 hrs 45 minutes. The blade sections were tested using a maximum design load and were found to be structurally adequate. However, due to the lack of sufficient resolution of the 3D printer, a significant post processing was required machining grooves for supporting rods. It was suggested to use a machine with more resolution for future attempts (B. K. Post et al., 2018).

*Figure 2.11: The adopted XZERES 442SR wind turbine (above) and the 3D printed blade sections (below) (B. K. Post et al., 2018)*

Another Partnership between ORNL and TPI composites aimed at building a 13 m long wind turbine mold. It was thought that using 3D printing would reduce the time and cost of producing wind turbine molds. The BAAM system used was 1000 times faster than desktop 3D printers capable of printing more than 4,500 $mm^3/s$ and had a workspace 2.4 m wide, 6.1 m long, and 1.8 m high. The material used was pelletized carbon fiber reinforced thermoplastic which was 100 times cheaper than other alternatives. The mold, shown in figure 2.12, contained channels for heating reducing the assembly time of the heating system drastically. The vacuum integrity, surface characteristics, mold distortion, and temperature gradient were tested and found to be sufficient for low volume production. The researchers also state that while it is not feasible to print large wind turbine blades currently, developments in Additive Manufacturing can make it possible in the future (B. Post et al., 2017).

*Figure 2.12: Final molds produced, upper and lower sections (B. Post et al., 2017)*

In another work, researchers at Nelson Mandela Metropolitan University, South Africa investigated three structural approaches utilizing 3D printing. A custom 3D printer was designed and manufactured based on the Prusa I3 3D printer. PLA was used to print the blade due to its better thermal expansion properties. First the printed blade was completely hollow, and an epoxy-glass-micro-balloon mix was cast inside the shell. Second, a hollow printed blade was filled with loose short strand fiberglass and infused with epoxy resin. Third, the blade was printed with an internal lattice structure and in the hollow space were inserted pultruded fiberglass rods which were tied to the printed structure with epoxy casts at the root and tip. The printer and the various approaches used are shown in figure 2.13.

In total, 3 blades could be produced with these methods in 5 – 7 days. The blades cost between 150 – 500 ZAR. Testing of the blades was performed up to wind speeds of 9 m/s and over rotational speeds of 500 rpm in a wind tunnel. The third approach was found to be the most favorable in terms of geometric accuracy and weight (Poole & Phillips, 2015).

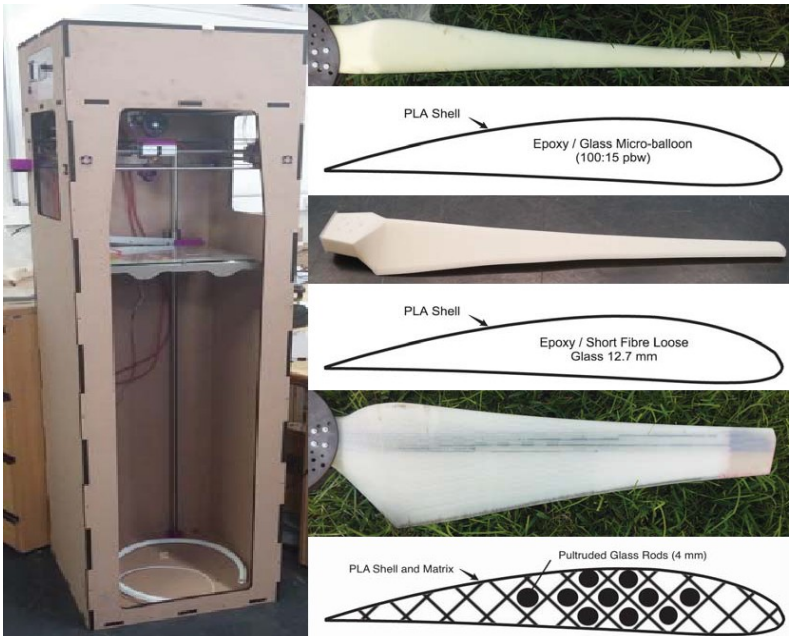


*Figure 2.13: The 3D printer used (left) and the three methods used (right) (Poole & Phillips, 2015)*

Akour et al. looked at the wind profiles of two cities in the UAE, Abu Dhabi and Al Ain to obtain an optimized geometry. Three airfoils BW3, A18, and SG6043 were selected for the optimization. BEM theory was used during the optimization, and the performance of the final geometry was analyzed using Qblade. The prototype blade was 3d printed using a XYZ Da Vinci 1.0 3D printer. The 55 cm blade was divided into four parts and printed. The blades were swapped with the blades of a 400 W AIR-X turbine, shown in figure 2.14, and tested in an outdoor environment. The results showed that the new rotors were more efficient below 11.5 m/s (Akour et al., 2018).


*Figure 2.14: 3D printed blades on an AIR-X generator (Akour et al., 2018)*

## 2.9. Cost Modeling of Wind Turbines

The cost of production processes can be analyzed in two ways: using cost estimators or using cost models. Cost estimators are used to find out an accurate and precise total cost of a production process. Thus the emphasis of cost estimators is on the predicted cost of the process. On the other hand, cost models, in addition to providing good final cost estimates, are used to find out the relationship between the cost and various factors that affect the process. Thus cost models can be used to make design decisions that minimize the cost of the part to be produced. When it comes to the modeling of Additive Manufacturing processes for example, cost models can be used to compare the cost of traditional manufacturing methods with AM processes and choose a process. An AM cost model can also be used to find the parameters that result in the lowest cost of production (Bernard et al., 2019).

There are three types of cost modeling techniques that are applicable to any manufacturing process. These are intuitive, analogical, and analytical cost modeling techniques (Busachi et al., 2017). A fourth one, parametric methods, is sometimes mentioned in the literature (Bernard et al., 2019).

Intuitive modeling techniques use data available in a database of past designs to make design decisions on new designs that are known to be closely related. In case of a significant difference, more data needs to be collected to fill the gap. It has been observed that better accuracy is obtained using these techniques when the attributes of the design are prioritized based on their impact. Three methods are typically employed: rule-based systems, fuzzy logic systems, and expert systems. Rule-based systems use time and cost calculations to choose from possible processes. Fuzzy logic systems are used to deal with uncertainty in simple models of manufacturing processes and yield better accuracy. Expert systems simulate a real human expert by storing and logically manipulating expert knowledge.

Analogical methods try to obtain statistical relationships between variables and cost using past data and predict the cost of new designs. Significant variables are identified and Cost Estimation Relationships (CERs) are generated to predict the total cost. In general, in order for this method to work, the variables and the cost must have a linear relationship and the variables must be independent. However, Artificial Neural Networks (ANNs) have been used successfully to obtain these relationships among non-linear variables using little data. ANNs also don’t require detailed process or product characterization. Parametric methods are similar to analogical methods, but the CERs take the form of mathematical functions containing all the variables. Tolerance-based costing relates the cost to the design tolerances of the product.

Activity-based costing goes a step further by estimating the time required and assigning overhead costs proportionally for each activity in the process. Then indirect costs can for each activity can be found by multiplying the cost rate by the time. Indirect costs are costs that are a function of time, like labor costs, maintenance costs, consumables, machine deprecation cost, space rent and overheads. The direct costs, which mainly include raw material costs, depend on the volume of the product. The total cost is then found by adding the direct and indirect costs (Bernard et al., 2019).

There are several types of analytical methods. Feature-based costing relates the features of products to their associated costs. This method is not flexible and is seldom used. Operation-based costing consists of identifying the activities involved in a production process and assigning times for each of them. This method performs well when detailed information about the production processes is available such as in the final design stages.

Of these techniques, parametric techniques and activity-based estimation are used widely in the literature. Parametric techniques do not require deep knowledge about the process. On the contrary, activity-based cost models are built using a detailed understanding of the products, processes and all the operations, components, and activities relating to them (Bernard et al., 2019). Thus they can provide an accurate, consistent, and robust means of cost characterization.

## 2.10. Optimization of Wind Turbines

The important optimization objectives found in the literature are coefficient of power, annual energy production, and cost of energy. A few others are sometimes employed like rotor thrust and blade mass (Chehouri et al., 2015). The objectives are the quantities to be maximized or minimized in the optimization. Cost-of-energy optimization is key because it minimizes the cost of producing a unit of energy. It is the annual cost divided by the annual energy production.

Multi-objective optimization takes into consideration more than one objective. This can be important in hitting multiple goals at once. When the objectives are conflicting, which is often the case, Pareto optimization is used to identify a set of solutions where maximizing one objective negatively affects at least one other objective. There are also other ways of approaching multi-objective optimization like simply weighting each objective and adding them to obtain a single composite objective (Chehouri et al., 2015).

The scope of optimization is also subject to variation. In airfoil shape optimization, blade parameters such as chord and twist distribution are held fixed while the shape of the airfoil is optimized. In blade performance optimization, the opposite happens where the airfoil shape is fixed and the blade parameters are allowed to vary. Another type of optimization is total wind turbine

optimization. This takes into account all blade parameters as well as all the other wind turbine components, the nacelle, and the structure. This is essential in cost-of-energy optimization as the forces experienced on the blade affect these components and these components contribute a big portion to the total cost of the turbine (Chehouri et al., 2015).

There are a lot of design constraints that can be employed. These constraints, broadly classified as geometric, aerodynamic, and physical constraints, serve in limiting the design space to feasible designs that we actually care about (Chehouri et al., 2015).

Optimization algorithms can be grouped as gradient-based algorithms (GBAs) and metaheuristic algorithms (Chehouri et al., 2015). Gradient-based algorithms are a class of algorithms that use gradient information to find the optimum solution. Some examples are gradient descent and Newton's method. Metaheuristic algorithms are usually non-deterministic algorithms that utilize simple rules to efficiently search the parameter space.

Among metaheuristic algorithms, genetic algorithms (GAs) have been widely utilized for wind turbine optimization. Genetic algorithms seek to find a good solution by selecting the best members of a design population and allowing them to "reproduce". Through this selection process and an added random mutation, each successive generation gradually performs better and better. GAs are better at locating neighborhoods of global optima than GBAs. They can also work with discrete as well as continuous parameters, whereas GBAs can only work with continuous and differentiable variables. In addition, they produce a population of solutions which makes them less sensitive to the initial configuration. However, they take a long time to converge to the actual solution. Moreover, they do not support separate constraints, and constraints have to be added to the objective as penalty functions. Since GBAs are relatively fast at searching for local optima, a hybrid algorithm that uses both approaches has been demonstrated to yield better results. Another metaheuristic algorithm called particle swarm optimization has also been utilized although not as widely (Chehouri et al., 2015).

A few optimization programs are available for the design of wind turbines. PROPGA is a hybrid genetic algorithm design tool for the design of HAWTs. It combines a genetic algorithm with an inverse design tool (Selig & Coverstone-Carroll, 1996). HARP_Opt (Horizontal Axis Rotor Performance Optimization) is another software has been used in the design of HAWTs. It uses a multi-objective genetic algorithm together with a blade element momentum model for the design of wind turbine as well as hydrokinetic turbine rotors (Sale, 2010).

# Chapter 3. Methodology

## 3.1. Overview

This research questions broadly whether additive manufacturing has the potential to reduce cost prediction error and thus be used in wind turbine manufacturing. Specifically, it is sought to ascertain whether the relative ease with which the cost of additive manufacturing can be mathematically modeled presents an opportunity for the cost of energy optimization of wind turbine blades.

Even though several works that investigate cost modeling of FDM printing have already been published (Alexander et al., 1998; Bernard et al., 2019; Costabile et al., 2017; Kadir et al., 2020), beyond general formulae, specific formulae, usable for any situation, have not been found. This is understandable as the cost depends on a multitude of factors including machine type, part complexity, operating parameters and operator skill that are impossible to formulate for all cases. Thus, it was deemed prudent to employ a hands-on approach and model the cost from experience while still using the guidelines of previous works.

A cost model is built by using activity based estimation, which divides the whole process into a series of activities and estimates the cost. Constants like indirect cost rates are situation dependent so a trial print is performed to ascertain all parameters in the formulation.

The cost model is then used in an optimization program developed to optimize the cost of energy. This program uses a genetic algorithm to obtain a population of superior designs. The variables used in the optimization are the airfoil sections used, design tip speed ratio, and design wind speed. The lift and drag coefficients for the airfoils were obtained from Prof. Michael Selig's website at the university of Illinois (Michael Selig, 2024).

The program used blade element momentum analysis to obtain the annual energy production and the cost of energy. Besides simple analysis, the BEM program also chooses the twist distribution of the turbine so that the lift to drag ratio at every section is minimized at the optimum velocity. Thus, the turbine performs best at this optimum velocity.

Wind data is input using Weibull probability distribution parameters. For this work parameters for Addis Ababa were taken ($\lambda = 4.24, k = 2.01$) (Bekele & Palm, 2009), but analysis can be done for any location by changing these parameters.

The power output is assumed to be limited once the wind turbine experiences enough wind speed to generate the rated power. This control is assumed to be provided by a circuit that varies the generator constant so that the speed is adjusted in such a way the wind turbine power does not exceed the rated power. The steps followed in this research is shown in figure 3.1.

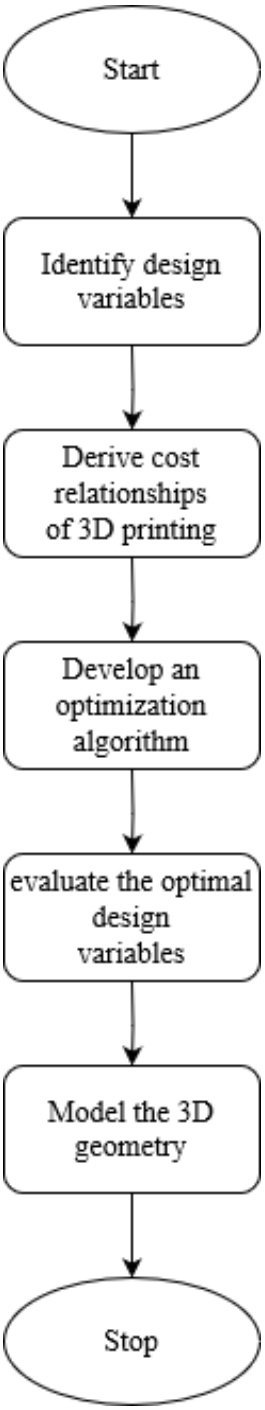


*Figure 3.1: Methodology flow chart*

This research falls in the category of exploratory research. The ultimate direction it aims to contribute to is proving that Additive Manufacturing possesses a greater potential for wind turbine blade manufacturing. It aims to do that by exploring ways of quantifying and optimizing additive manufacturing costs for wind turbine blades. However, the scope of this aim is very broad, and the effect of many other parameters must be explored before a definitive answer can be given. This research outlines the basic procedures to be followed for understanding the most important parameters.

## 3.2. Additive Manufacturing Cost Modeling

The cost model is built in five steps. First, the scope of the cost model is defined to be certain of the activities included. Then the formula for estimating the build time is laid down. Build time is essential because all indirect costs depend on the build time. The indirect cost rates are estimated followed by direct costs. Finally, all estimates are combined into a single relation that can be used in our optimization program to predict the cost of energy.

### 3.2.1. Definition of Scope

The first step in estimating the cost is specifying the scope of the cost model. The whole process can be broken down into three phases: pre-processing phase, build phase, and post-processing phase. The pre-processing phase comprises of file conversion, file transfer, and machine preparation. The post-processing phase contains product removal and surface processing (Bernard et al., 2019). In this research, all of these phases were investigated.

### 3.2.2. Build Time Estimation

The next step is to estimate the build time. Equation 3.1 – 3.6 are used for this purpose (Alexander et al., 1998).

$$T_{build} = \sum_{i=1}^{N_{lay}} t_{\mathrm{lay,i}} + N_{lay}\, t_{zmove} + \frac{N_{lay}}{m} t_{wipe} \tag{3.1}$$

$$t_{\mathrm{lay,i}} = t_{\mathrm{part,i}} + t_{\mathrm{supp,i}} + t_{\mathrm{move,i}} \tag{3.2}$$

$$t_{\mathrm{part,i}} = \frac{A_{\mathrm{part,i}}}{w_{part}\, v_n} \tag{3.3}$$

$$t_{\mathrm{supp,i}} = d\,\frac{A_{\mathrm{supp,i}}}{w_{supp}\, v_n} \tag{3.4}$$

$$d = \frac{w_{supp}}{w_{supp} + w_{gap}} \tag{3.5}$$

$$N_{lay} = \frac{H}{z_t} \tag{3.6}$$

Where

$T_{build}$ is the total build time,

$t_{\text{lay,i}}$ is the build time for the i$^{th}$ layer,

$N_{lay}$ is the number of layers,

$t_{zmove}$ is the time taken to move to a new height after a layer is finished,

$t_{wipe}$ is the time taken to wipe the head done every $m$ layers,

$t_{\text{part,i}}$ is the time taken to lay down part material for the i$^{th}$ layer,

$t_{\text{supp,i}}$ is the time taken to lay down support material for the i$^{th}$ layer,

$t_{\text{move,i}}$ is unproductive time spent moving between roads,

$A_{\text{part,i}}$ is the cross-sectional area taken up by the part material on the i$^{th}$ layer,

$w_{part}$ is the road width of the part material,

$v_n$ is the nozzle velocity in the x-y plane,

$A_{\text{supp,i}}$ is the cross-sectional area taken up by the support material on the i$^{th}$ layer,

$w_{supp}$ is the road width of the support material,

$w_{gap}$ is the gap between adjacent roads,

$d$ is the fraction of the support area filled with support material,

$H$ is the part height, and

$z_t$ is the layer thickness.

The calculation of $t_{\text{part,i}}$ assumes a constant nozzle velocity. But in actuality, the nozzle accelerates and decelerates. To account for this, a correction factor is applied as shown in equations 3.7 and 3.8.

$$t_{\text{part,i}} = \frac{A_{\text{part,i}}}{w_{part} v_n f} \tag{3.7}$$

$$f = \frac{A_{\text{sec,gen}}}{w_{part} v_n t_{\text{sec,gen}}} \tag{3.8}$$

Where

$f$ is the correction factor,

$A_{\text{sec,gen}}$ is the cross-sectional area of a generic airfoil, and

$t_{\text{sec,gen}}$ is the actual time taken to print the generic airfoil section.

The final calculation of the build time can be simplified because we know that the chord of each section varies linearly with height. In addition, we also know that only the first few layers will have support in the form of either a brim or a raft whose area depends on the base area of the part. One assumption we make is that the airfoil is printed in a spiral pattern and for each layer the start and end nozzle positions differ only by the shell thickness which we consider negligible. Therefore $t_{\text{move,i}}$ is negligible. The modified equation is shown in equation 3.9.

$$T_{build} = \left(t_{zmove} + \frac{t_{wipe}}{m} + \frac{t_{\text{part,1}} + t_{\text{part,n}} + \sqrt{t_{\text{part,1}} t_{\text{part,n}}}}{3}\right) N_{lay} + t_{\text{lay,supp}} N_{supp} \tag{3.9}$$

Where

$t_{\text{part,1}}$ and $t_{\text{part,n}}$ are the time taken to print the bottom and top part layers respectively,

$N_{supp}$ is the number of support layers, and

$t_{\text{lay,supp}}$ is the time required to print the support layer.

To use the above equations, first the printer specifications and settings must be known. Specifically, print area dimensions, layer thickness, nozzle velocity, and road thickness must be known. The operator was consulted to find out that $t_{zmove}$, $t_{wipe}$, $m$, were insignificant. Additionally, due to the favorable geometry of the blades, no support structures are needed. Then the expression for $T_{build}$ can then shown as in equation 3.10.

$$T_{build} = \left(\frac{A_{\text{part,1}} + A_{\text{part,n}} + \sqrt{A_{\text{part,1}} A_{\text{part,n}}}}{3 w_{part} v_n f}\right) \frac{R}{z_t} = \frac{V}{w_{part} v_n f z_t} \tag{3.10}$$

Where $V$ is the volume. It can be seen that $T_{build}$ is directly proportional to the volume of the part, which intuitive.

### 3.2.3. Indirect Cost Rate

The components of indirect cost include machine deprecation cost, maintenance and consumables, labor cost, and overhead cost (manufacturing space, administrative costs, computers, communications, software licenses, and energy).

The machine deprecation cost depends on the machine capital cost and the lifetime of the printer. Its formula is shown in equation 3.11. The computer cost rate is calculated with the same formula.

$$\dot{C}_{depr} = \frac{C_{prntr}}{L_{prntr}} = \frac{170\,\$}{7500\,hrs} = 2.3\,Birr/hr \tag{3.11}$$

Where

$\dot{C}_{depr}$ is the deprecation cost rate,

$C_{prntr}$ is the printer cost, and

$L_{prntr}$ is the life of the printer.

The maintenance cost is calculated from the annual maintenance cost and the yearly operating hours as shown in equation 3.12.

$$\dot{C}_{mnt} = \frac{C_{\text{mnt,ann}}}{8760\,hrs/yr\,cf} = \frac{25\,\$/yr}{8760\,hrs/yr\,0.7} = 0.41\,Birr/hr \tag{3.12}$$

Where

$\dot{C}_{mnt}$ is the maintenance cost rate, and

$C_{\text{mnt,ann}}$ is the annual maintenance cost.

The hourly labor cost was estimated from data published by the International Labor Organization for a medium skill level (*ILOSTAT Data Explorer*, n.d.). The most recent data was for 2021 and the value was adjusted for inflation. The value obtained for the end of 2023 is 29 Birr/hr. The operator is assumed to work regular hours, 8 hrs per day, 22 days per month. Therefore, the labor cost must be converted to per total time instead of just working hours. The 3d printer is assumed to work all hours when it is not down for repairs. This final labor cost rate is calculated as in equation 3.13.

$$\dot{C}_{\text{oper}} = \frac{\dot{C}_{normal}\,Hrs_{working}}{Hrs_{total}\,cf} = \frac{29\,Birr/hr \cdot 8\,hrs/day \cdot 22\,days/month}{24\,hrs/day \cdot 30\,days/month \cdot 0.7} = 10\,Birr/hr \tag{3.13}$$

The rent of the manufacturing space is estimated 20,000 Birr/month. Including in the capacity factor in the analysis the space cost rate can be found as shown in equation 3.14.

$$\dot{C}_{space} = \frac{rent}{72\,hrs/month\,cf} = \frac{20000\,Birr/month}{720\,hrs/month\,0.7} = 40\,Birr/hr \tag{3.14}$$

### 3.2.4. Direct costs

Direct costs are mainly concerned with the material used in printing. The cost per part can be found by multiplying the price per unit volume of the print material with the volume of the part.

### 3.2.5. Pre-processing cost

The pre-processing cost can be assigned indirect cost rates just like the build cost as shown in equation 3.15 (Alexander et al., 1998).

$$C_{pre} = T_{pre}\left(\dot{C}_{\text{oper1}} + \dot{C}_{comp}\right) + T_{setup}\dot{C}_{\text{oper1}} \tag{3.15}$$

Where

$C_{pre}$ is the pre-processing cost,

$T_{pre}$ is the pre-processing time determined from observation,

$\dot{C}_{\text{oper1}}$ is the operator labor cost rate,

$\dot{C}_{comp}$ is the deprecation cost of the computer system used, and

$T_{setup}$ is the time required to setup the machine.

However, the time it takes has been observed to be insignificant when compared to the build time. Thus the whole pre-processing cost is ignored with the exception of the computer deprecation cost. Since the estimate of life of the computer system is not based on the pre-processing time, it might need to idle between use or serve other purposes, the entire time between the start of successive part prints is used. This introduces a capacity utilization factor, which is the amount of time per year the printer is operational. The capacity factor is assumed to be 0.7, an average capacity factor for 3D printing systems (Bernard et al., 2019). Due to these assumptions, the expression for the pre-processing cost is modified to equation 3.16.

$$C_{pre} = \frac{\dot{C}_{comp}\,T_{build}}{cf} \tag{3.16}$$

Where

$cf$ is the capacity utilization factor.

### 3.2.6. Post-processing cost

Similarly, the post-processing cost can be calculated using indirect cost rates as in equation 3.17 (Alexander et al., 1998).

$$C_{post} = (T_{rem} + T_{fin})\dot{C}_{oper2} + C_{ppmat} A_{surf} \quad (3.17)$$

Where

$C_{post}$ is the post-processing cost,

$T_{rem}$ is time required to remove the part,

$T_{fin}$ is the time required for surface finishing of the part, and

$\dot{C}_{oper2}$ is operator cost for post-processing.

Here, it is assumed that the build time is more than the post-processing time. Therefore post-processing activities of a part may be done while the next part is being printed, with the same operator manning the print as well as doing the post-processing. The post-process activity is wet sanding with fine grit sandpaper followed by coating the part with epoxy resin to achieve a similar surface finish to the test pieces used to generate the airfoil data (Selig, 1995). A 1 mm coat of epoxy is assumed. Thus the expression for the post-processing cost is simplified to equation 3.18.

$$C_{post} = C_{ppmat} A_{surf} \quad (3.18)$$

### 3.2.7. Virtual Factory

Some assumptions were made about the manufacturing setup so that some of the parameters in the formulas above can be determined. It is assumed that the factory is a small operation with a single printer and operator. This assumption simplifies the process of modeling but it can be revised in future works to determine if the cost can be further driven down by scaling up operations. Additionally, no administrative overhead is assumed due to the size of operation.

### 3.2.8. 3D Printer Specifications

The 3D printer used is the Creality Ender 3 v2 shown in figure 3.2. Its specifications are given below together with the process parameters.

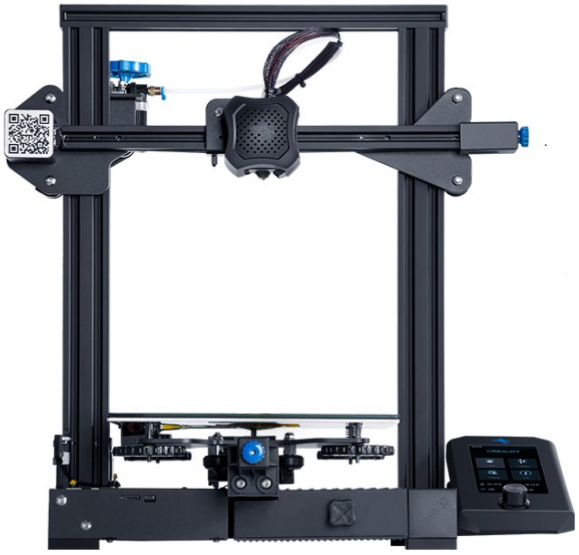

*Figure 3.2: The Ender 3 v2 3D printer*

### 3.2.9. 3D Printing Process Parameters

The printer and print settings in the slicer were examined to determine some parameters in the equations used above which are summarized in table 3.1. Together with the assumptions of our virtual factory it gives us a complete information to build our cost model. A slicer was used to get recommended print settings. The maximum print dimensions, layer thickness, nozzle velocity and road thickness (nozzle diameter) were obtained from the printer specifications and the recommended settings on the slicer. The indirect cost rates were estimated previously. The rationale behind the remaining parameters are explained below.

A sample airfoil cross-section was used to estimate the relationship between the theoretical and actual print times. A single layer of an airfoil shell was used for the test. The 3D model of the test airfoil section was imported into the slicer and the actual print time was thus obtained. The correction factor earlier is the ratio between this actual time and the theoretical time from equation 3.3.

*Table 3.1: Parameters used in cost modeling*

| Parameter | Required Data | Value |
|---|---|---|
| Printer height | | 250 mm |
| Max horizontal print dimension | Max thickness of airfoil (19 % of chord) | 260 mm |
| Layer thickness, $z_t$ | | 0.2 mm |
| Nozzle velocity, $v_n$ | | 50 mm/s |
| Road thickness, $w_{part}$ | | 0.4 mm |
| Sample airfoil cross-section print time, $t_{\text{sec,gen}}$ | Total print time and number of layers | 108 sec |
| Sample airfoil cross-section area, $A_{\text{sec,gen}}$ | | 0.000958 $m^2$ |
| correction factor, $f$ | $t_{\text{sec,gen}}$, $A_{\text{sec,gen}}$, $v_n$, $w_{part}$ | 0.44 |
| Deprecation cost rate | Printer cost and life | 2.3 Birr/hr |
| Maintenance cost rate | | 0.41 Birr/hr |
| Labor cost rate | | 10 Birr/hr |
| Computer and software cost rate | Computer and software cost and life | 1.4 Birr/hr |
| Energy cost rate | Power used and energy cost | 0.743 Birr/hr |
| Post-processing material cost per area | Primer and paint cost per volume and coating thickness | 400 Birr/$m^2$ |
| Manufacturing space rent | Space required and rent prices | 40 Birr/hr |
| PLA price per unit volume | Price per unit mass and material density | 7.31 Birr/$cm^3$ |

Thus the total cost for a part is given in equation 3.19.

$$C_{tot} = \left(\dot{C}_{comp}/cf + \dot{C}_{depr} + \dot{C}_{mnt} + \dot{C}_{\text{oper}} + \dot{C}_{en} + \dot{C}_{space}\right) T_{build} + PPV \cdot V + C_{ppmat} A_{surf} \quad (3.19)$$

Where

$C_{tot}$ is the total cost,

$C_{depr}$ is the deprecation cost rate,

$C_{mnt}$ is the maintenance cost rate,

$C_{en}$ is the energy cost rate,

$PPV$ is the price per volume of the print material, and

$V$ is the volume of the part.

The cost can now be written as a linear function of the volume. An average shell thickness can be prescribed below which the blade becomes structurally compromised. The cost is then written as in equation 3.20 and the finally as equation 3.21.

$$C_{tot}=\left(\frac{\dot{C}_{comp}/cf+\dot{C}_{depr}+\dot{C}_{mnt}+\dot{C}_{\text{oper}}+\dot{C}_{en}+\dot{C}_{space}}{w_{part}\,v_n f\,z_t}+PPV+C_{ppmat}/t_{sh}\right)V \tag{3.20}$$

Where

$t_{sh}$ is the shell thickness.

$$C_{tot}=\left(1.61\times10^{7}+400/t_{sh}\right)V \tag{3.21}$$

From this we can see that the shell thickness can be as small as 1 mm and the second term will still be negligible. Therefore we drop it and perform our optimization based on the linear relationship only.

### 3.2.10. Cost of Other Components

The cost of the generator, tower, yaw and furling system, control system, balance of system, etc are all assumed constant for a chosen rated power. Thus, they won't significantly affect the result of the optimization. Once a cost of energy has been formulated based on the cost of the blades, this can be scaled up to an estimate of the cost of energy based on the entire turbine. This is because the blades are known to cost around 7 % of the total cost of the turbine for small wind turbines (Wood, 2011). This results in the cost of the turbine being expressed as equation 3.22.

$$TC=1.61\times10^{7}V/0.07=2.29\times10^{8}V\ Birr/m^{3} \tag{3.22}$$

## 3.3. Benchmark design

The Skystream 3.7 wind turbine, shown below in figure 3.3, was chosen as a benchmark so that the performance of the optimized design can be compared to it. The maximum power of the optimized design was chosen to be similar to this benchmark. The turbine costs $19,000 (adjusted for inflation) including installation (*Wind Turbines Comparison 2009*, n.d.). This turbine is estimated to produce 4,406 MJ (1,224 Kwh) of energy annually in Addis Ababa. This value is obtained from the power curve of the turbine and the wind distribution of our design location. The power curve of the turbine is shown in figure 3.4.

*Figure 3.3: The Skystream 3.7 (Small Turbine Product Reviews, n.d.)*

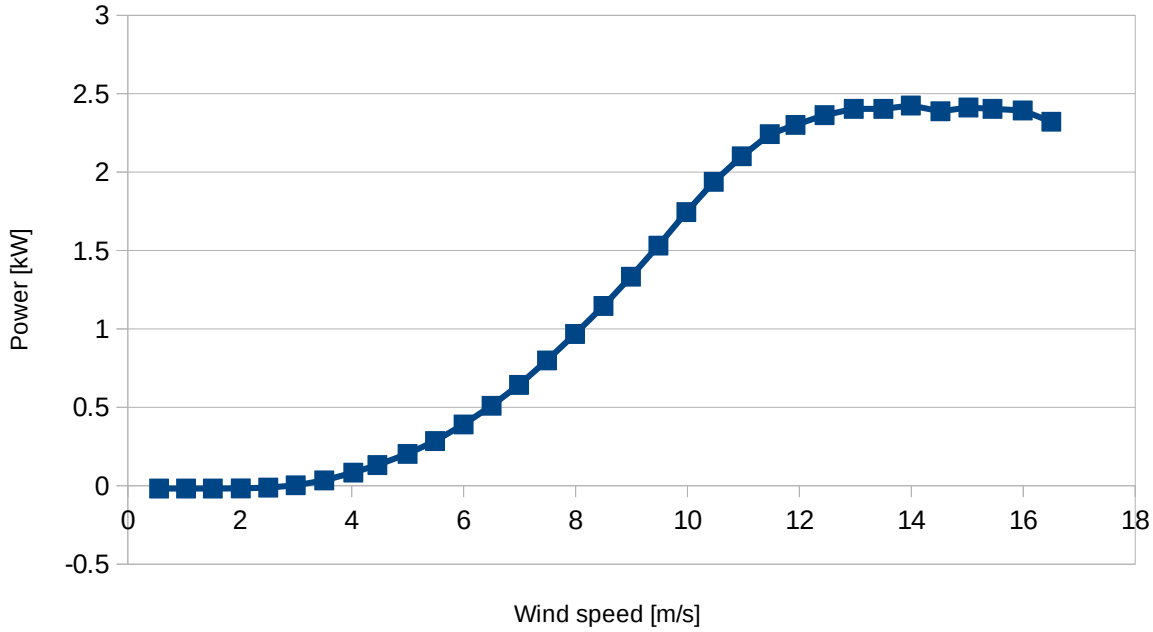


*Figure 3.4: Power curve of the Skystream 3.7 (XzeresSkystream3.7_2.1kW_3.7 — NREL/Turbine-Models Power Curve Archive 0 Documentation, n.d.)*

## 3.4. Airfoil Polar Data Collection

Experimental data for lift and drag coefficients were obtained from Prof. Michael Selig's website at the university of Illinois (Michael Selig, 2024). The tests were performed in wind tunnels at the low Reynolds numbers (<500,000) suitable for small wind turbines. Coordinate files for these airfoils were also obtained from the same site which was used to calculate the section areas and section moduli. Airfoils specifically used for wind turbines were chosen among this database. These were the SG6040 and BW-3 for the root-ward sections and the SG6041, SG6042, SG6043, USNPS-4 and SD7062 airfoils.

The data was in the form of multiple text files which were published separately and had different formats in some cases. These files were organized into a python dictionary for use in the optimization program. Then an interpolating code was written to interpolate coefficients at permissible angles of attack and any Reynolds number. The data contains coefficients only for small angles of attack. For angles whose absolute values exceed the upper data limit, equations 3.23 and 3.24 are adopted (Wood, 2011).

$$c_l = 2\sin\alpha\cos\alpha \tag{3.23}$$

$$c_d = 2\sin^2\alpha \tag{3.24}$$

This approximation is thought to be acceptable because at angles that exceed the maximum angle in the data, the airfoil is thought to have already stalled and the program will give a conservative estimate of the performance of the turbine. For angles lower than the data range, the linear trend is assumed to continue up to the negative of the upper angle limit. This way the program underestimates the performance even if the airfoil stalls in that range. The drag in this range is taken to be the drag at the upper data limit which also ensures a conservative analysis.

The Reynolds numbers are not interpolated directly. Instead, their logarithms are interpolated (Wood, 2011). If the Reynolds number falls outside the data provided, the data at the nearest extreme point is used.

## 3.5. Optimization Program

The program uses a genetic algorithm to find designs with a relatively good cost of energy. The genetic algorithm produces populations of designs whose performance improves as the iteration progresses. This improvement is due to crossover, selection, and mutation that are present in any evolutionary process. The “genes” of each design code for a design’s tip and root chord (a linear distribution is assumed between them), airfoil sections, number of blades, design wind speed, and the design tip speed ratio. The general workings of this program is shown below in figure 3.5. Each step in the algorithm is then described.

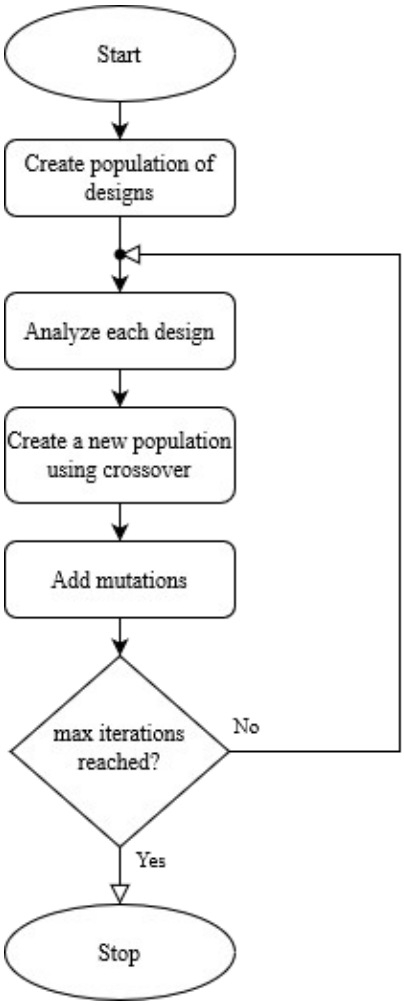


*Figure 3.5: Flowchart of genetic optimization algorithm*

### 3.5.1. Creating a Population of Designs

A population is a specified number of designs that are used to make a new generation of better designs. The size of the population allows there to be a lot of diversity in the designs and allows the program to get better results within fewer generations. However, as the population size is increased, creating each successive generation takes more time. The population size and number of iterations were calibrated so that the program could finish in a reasonable amount of time.

### 3.5.2. Analyzing Designs

Once a candidate design is created, randomly at first or by crossing over well performing designs from a previous generation, the objective has to be calculated. A blade element momentum code is used to calculate the AEP. Then the COE is obtained from the AEP and the cost model.

An important parameter that determines the size of the wind turbine is the rated power. This is chosen so that the results of the optimization can be compared with an established design, as

mentioned above. The maximum power of 2400W of the Skystream 3.7 was therefore used in our optimization.

The twist of the turbine is determined so that the twist that maximizes the lift-to-drag ratio at each blade section at the design wind speed. The twists obtained for the design wind speed are used in another analysis to determine the performance of the turbine across a range of operational wind speeds.

The range of wind speeds used in the analysis is between the cut-in and cut-out wind speeds. A rough value of 3.5 m/s was taken for the cut-in speed based on observations of existing designs. A more detailed analysis of starting performance is one area this work can be improved. The cut-out wind speed was taken to be the speed for which the probability there is going to be a wind speed above it is 0.001%. This probability is calculated using the cumulative Weibull probability distribution.

The stress is calculated based on the assumption that the blade is a beam with a shell cross-section. The bending and shear stresses are combined and a static Von-Mises criterion is used to determine failure. The stress is calculated at each section and for all design speeds and encountered wind speeds. An excessive stress is not cause to disregard the design altogether. In such an event a penalty proportional to the stress exceeding the allowable limit is added so that the design can possibly pass off advantageous attributes.

As previously mentioned there are two airfoils to be used in each design. It is known that most of the aerodynamic performance is dictated by tip ward sections, and most of the stresses arise in the root ward sections. Thus by having separate sections for the tip and the root, it is thought that a good design can be performs well on both counts.

Some constraints were placed on the parameters so that the program does not spend time analyzing unrealistic designs. The design tip speed ratio ranges from 3 to 9, which includes most commonly used tip speed ratios for the number of blades used (Carriveau, 2011). The design wind speed is constrained to lie between the cut-in and cut-out wind speeds. The working of the analysis program is shown in the flowchart in figure 3.4. The types of airfoils used were limited to those with a demonstrated performance when used in wind turbines.

The number of blades in most commercial wind turbines is three. Two bladed turbines seem cost effective at first glance, but they have a structural handicap. There is a wobbling created by the gyroscopic precession of the blades as the turbine yaws. More than three blades is of course even

less cost effective. The program, however, cannot perform such a sophisticated structural analysis. So the number of blades was fixed at three for all candidate designs.

The operating tip speed ratio is controlled by modulating the generator torque. This is known as Maximum Power Point Tracking (MPPT). Even after the rated speed is exceeded (the rated speed is defined here as the speed at which the power output becomes equal to the rated power) torque control is used to keep the power output below the rated power. Stall control is not possible because the stall data used is merely an approximation. And pitch regulation is seldom used in small wind turbines because of its cost.

### 3.5.3. Selection and Crossover

Crossover refers to the exchange of genes between the chromosomes of parents to make new genetic material for a child. In a similar manner, best performing members of a population of design are chosen so that they can "reproduce" in this manner. A simple average is taken of the attributes of the parents to create a new child.

Selection of the parents allowed to reproduce is key. Individuals with a good fitness, i.e. a good cost of energy, have a higher probability to reproduce.

### 3.5.4. Mutation

It is not enough that the best designs keep reproducing. Once in a while there needs to be a random mutation in the designs to stop the process from converging to a local minimum soon. While the algorithm is not guaranteed to converge to a global minimum, the results obtained get better over time.

The rate of mutation is an important parameter that affects how fast the program can give good results. If it is too little, the population becomes stagnant soon and not much change happens. If the mutation rate is too high the process resembles a random selection process that is chaotic and will likely not find good solutions, although the search area will be higher. Trial runs with small population sizes and numbers of iteration were performed. The best results were found for a mutation rate of 0.1.

To take advantage of both high and low mutation rates, the first half of the optimization was conducted with a mutation rate of 0.1, and the second half was conducted with a high mutation rate of 0.5. The results of the first half will persist even if the second half doesn't find a better solution.

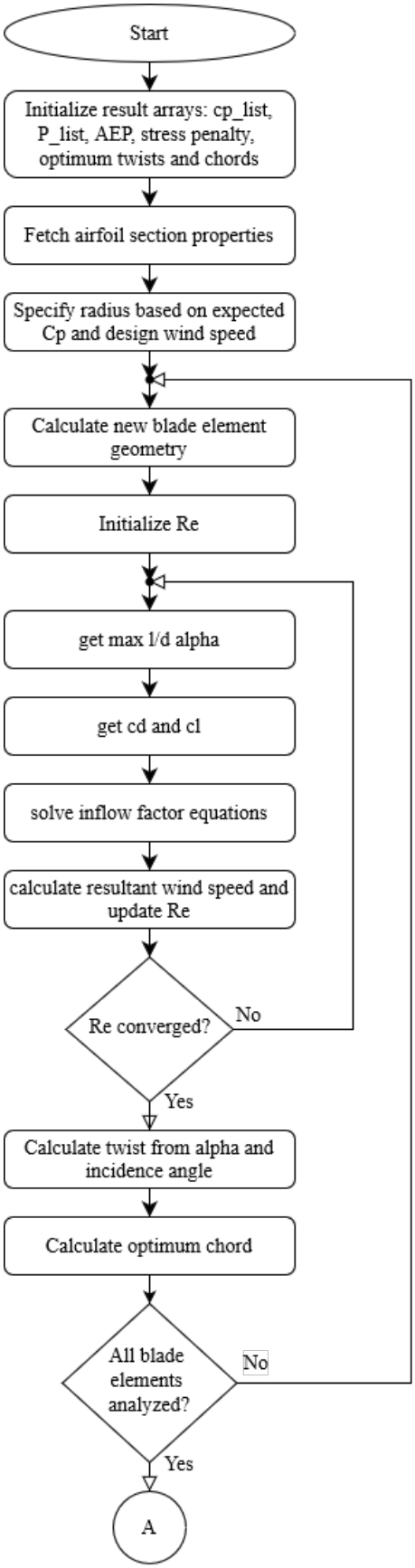


*Figure 3.6: Flow chart of the blade element momentum analysis program*

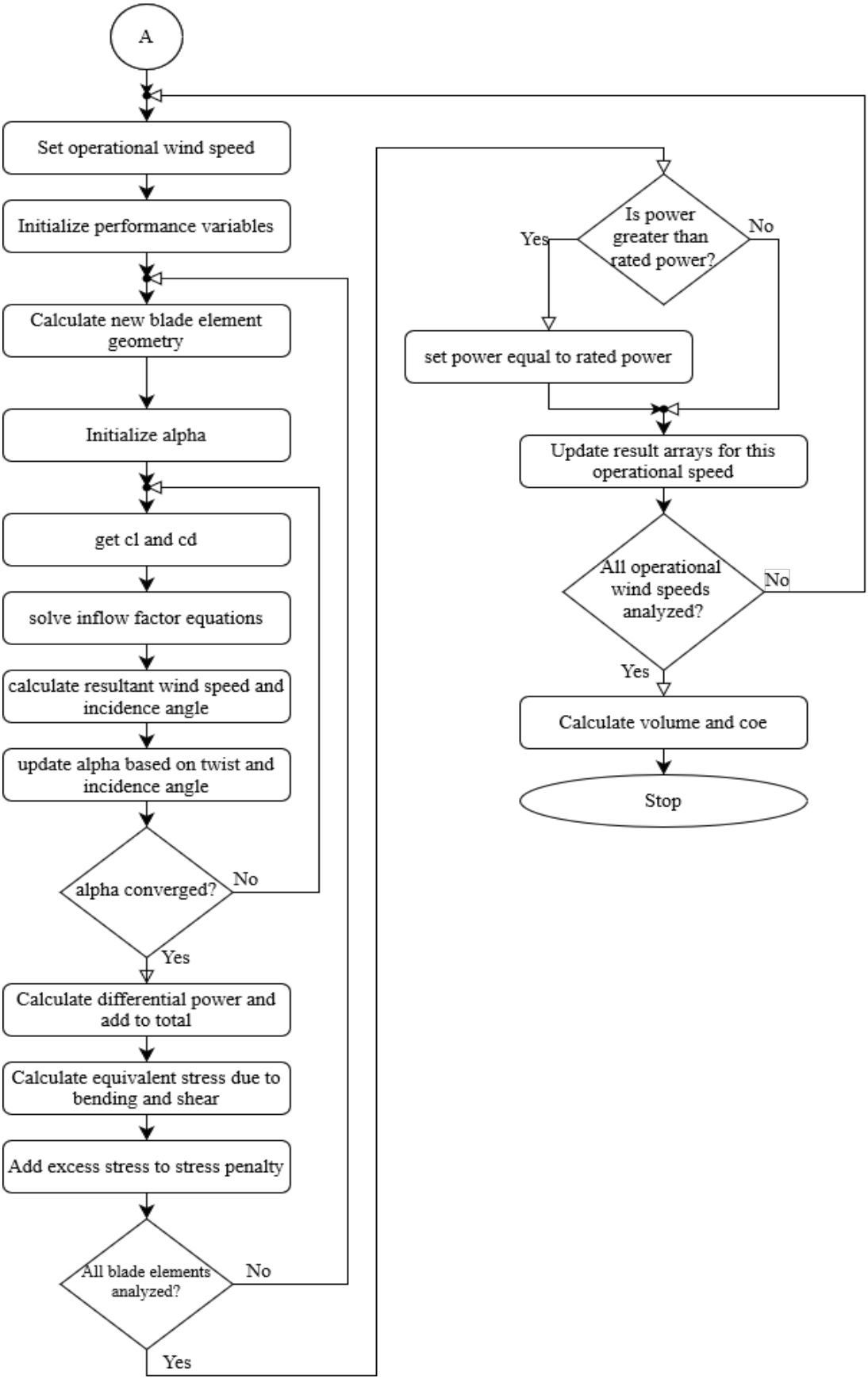


*Figure 3.7: Flow chart of the blade element momentum analysis program (cont.)*

# Chapter 4. Results and Discussion

## 4.1. Optimization Results

The program was run for 1000 iterations with a population size of 200. From previous runs, this setting was known to yield good results. With more iterations the program can give better solutions. The input parameters are shown in table 4.1 and the optimal design variables, objective and other relevant parameters of the optimal design are shown in table 4.2. The 3D model of the design is shown in figure 4.1.

*Table 4.1: Input parameters of the optimization*

| Parameter | Value |
|---|---|
| Wind distribution Weibull scale parameter (Addis Ababa) | 4.24 m/s |
| Wind distribution Weibull shape parameter (Addis Ababa) | 2.01 |
| Rated Power | 2400 W |

*Table 4.2: Result parameters of the optimized design*

| Parameter | Value |
|---|---|
| Root airfoil | SG6040 |
| Tip airfoil | SD7062 |
| Root chord | 165 mm |
| Tip chord | 39.5 mm |
| Design wind speed | 9.58 m/s |
| Design tip-speed ratio | 7.25 |
| Number of blades | 3 |
| Blade volume | $5.05 \times 10^{-3}$ m$^3$ |
| Annual energy production | 5,990 MJ |
| Volume per Annual energy production | $8.43 \times 10^{-13}$ m$^3$/J |
| Root twist | 59.2° |
| Tip twist | 88.6° |
| Maximum $C_p$ | 0.362 |
| Blade radius | 1,880 mm |

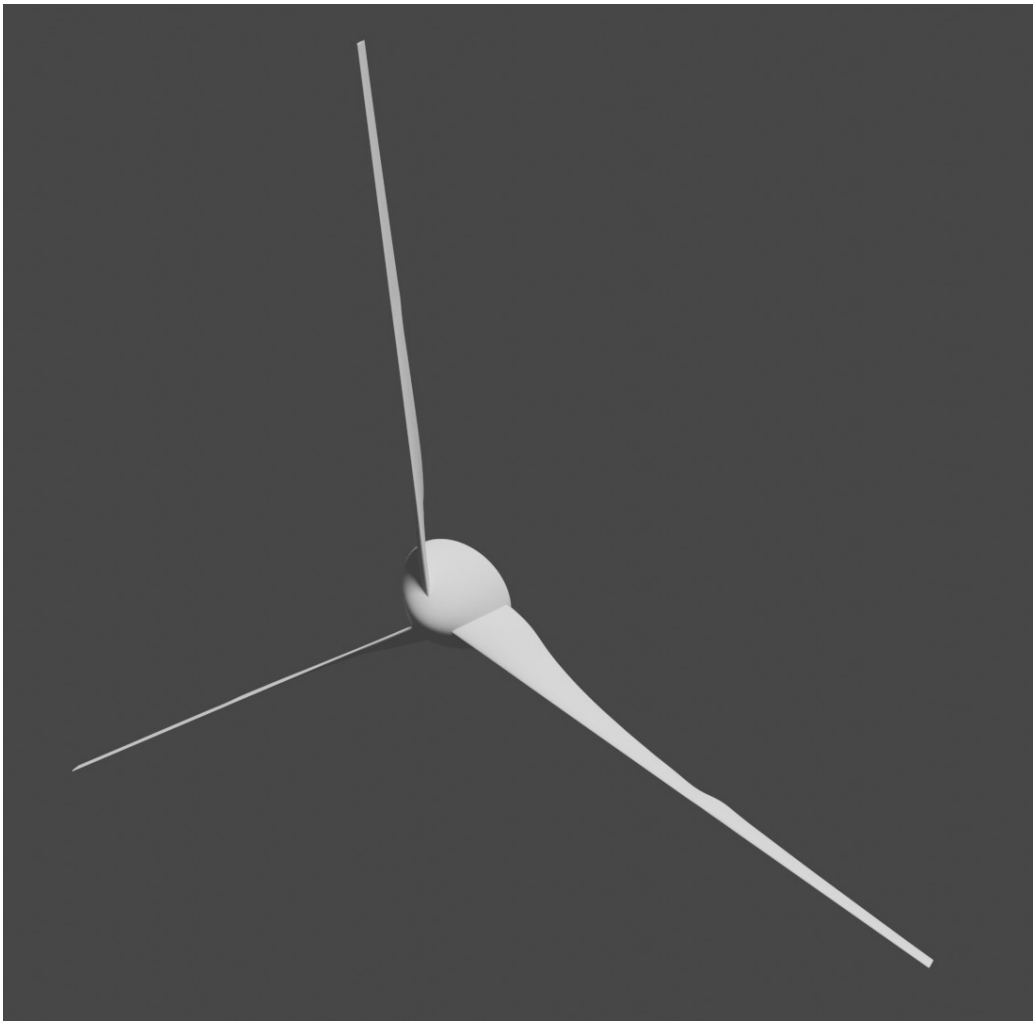

*Figure 4.1: A Rendering of the Design*

## 4.2. Discussion

The airfoils used for the root and tip were differentiated before being used. Therefore the program chose among root airfoils for sections closer to the root and tip airfoils for airfoils closer to the tip. The number of airfoils considered for each design was only two. But more number of designs are sure to increase performance.

The SG6040 airfoil used at the root is a member of the well known SG family of airfoils specifically developed for use in wind turbines. Similarly, the SD7062 was used in a 5kW variable speed wind turbine with good results (Lyon, 1997).

Another fact to note is that the design wind speed is greater than the mean or most likely wind speed for the chosen location. This is also in line with design principles. The power produced at higher wind speeds is much higher because of the cubic relationship between power and wind speed. This increase more than makes up for the unlikeliness of these higher wind speeds.

The design tip-speed ratio is also around the optimum dictated by the literature. For a wind turbine with 3 blades, the optimum tip-speed ratio is around 7 (Yurdusev et al., 2006).

The volume per AEP parameter mentioned here is a simplified version of the cost of energy. The actual cost of energy can be calculated from this value using the cost model established earlier. The yearly maintenance costs are assumed to be 3% of the capital cost (*Wind Turbines*, n.d.). The final cost of energy is shown in equation 4.1.

$$COE = \frac{FCR \times TC + OM}{AEP} = (0.03 + 0.0673) \times 2.29 \times 10^{8} \frac{V}{AEP} = 1.93 \times 10^{-5} \frac{Birr}{J} = 0.670 \frac{\$}{KWh} \quad (4.1)$$

This formula can also be used to obtain the cost of energy of the Skystream 3.7 as shown in equation 4.2.

$$COE = \frac{FCR \times TC + OM}{AEP} = (0.03 + 0.0673) \frac{19{,}000\,\$}{1224\,Kwh} = 1.51 \frac{\$}{KWh} \quad (4.2)$$

The twist increases swiftly at the root as the inflow angle changes rapidly at the root, which is what is seen in our result. The chord on the other hand is small compared to the radius of the blade yielding a rather high aspect ratio of 16. This results in a very slender blade which can be structurally unstable. Robust structural analysis must be performed to ascertain the structural soundness of such blades as opposed to the rudimentary analysis performed here. Such slender blades are to be expected when there are two competing objectives, the minimization of cost, and hence the volume, and the maximization of power production, and hence the blade radius. Since more power is produced at the outer regions of the blade, aerodynamic optimization tends to increase the radius.

The maximum coefficient of power of our design is higher than that of the benchmark design, 0.3, even though it was not the primary objective. Additionally, it is thought that with more run time better performing designs can be obtained.

## 4.3. Sensitivity Analysis

A sensitivity analysis is conducted to validate the results. The design variables, the tip-speed ratio, design wind speed, and airfoils used were perturbed and fed into the program. The main objective, the volume per AEP of each configuration was then compared with the previous result. The COE derived for each configuration is shown in table 4.3.

*Table 4.3: Results of sensitivity analysis*

| Parameter | Perturbation | | | | | | | | | |
|---|---|---|---|---|---|---|---|---|---|---|
| | -5% | -4% | -3% | -2% | -1% | 1% | 2% | 3% | 4% | 5% |
| COE for perturbed design tip-speed ratios | 0.79 $/Kwh | 0.77 $/Kwh | 0.74 $/Kwh | 0.72 $/Kwh | 0.69 $/Kwh | 0.65 $/Kwh | 0.63 $/Kwh | 0.61 $/Kwh | 0.59 $/Kwh | 0.57 $/Kwh |
| COE for perturbed design wind speeds | 0.67 $/Kwh | 0.67 $/Kwh | 0.67 $/Kwh | 0.67 $/Kwh | 0.67 $/Kwh | 0.67 $/Kwh | 0.67 $/Kwh | 0.68 $/Kwh | 0.68 $/Kwh | 0.68 $/Kwh |
| COE for BW-3 root airfoil | 0.72 $/Kwh | | | | | | | | | |
| COE for SG6041 tip airfoil | 0.79 $/Kwh | | | | | | | | | |
| COE for SG6042 tip airfoil | 0.66 $/Kwh | | | | | | | | | |
| COE for SG6043 tip airfoil | 0.60 $/Kwh | | | | | | | | | |
| COE for USNPS-4 tip airfoil | 0.69 $/Kwh | | | | | | | | | |

The red cells indicate that the configuration is invalid because the stress is above the allowed value. The green cells on the other hand have a stress value below the allowed value.

It can be seen that the valid results always have a higher cost of energy than our optimal value. Therefore we can say with reasonable certainty that our value is at least locally optimal. We can also deduce that while the objective is not very sensitive to the design wind speed, it is very sensitive to the tip-speed ratio. Therefore fixing the design wind speed at a reasonable value to make the optimization faster is a plausible alternative.

# Chapter 5. Conclusion

This thesis examined the cost of energy optimization of 3d printed wind turbine blades. For this purpose, a cost model was built. The modeling indicated that the cost is linearly related to the volume of the blade. The impetus for this research was that manufacturing wind turbines using laminate layup and subsequent vacuum bagging, resin transfer molding or similar processes is hard to accurately model. This inaccuracy was mentioned as one cause why cost of energy optimization is not prevalent (Chehouri et al., 2015). This research showed that in contrast 3d printing offers a very simple cost model to use in optimization.

The cost model was built by considering all the activities that comprise the whole process. These are grouped into pre-processing, build and post processing costs. Each of these phases were examined and relations for each costs were found from the literature. Some modification was performed to apply it to the specific case of 3d printing a blade structure. Additionally, the 3d printer and its settings were chosen which allowed the specification of all the parameters in the relations. After teasing out insignificant costs, the blade cost was found to be linearly related to the volume.

Next, a cost of energy optimization was performed using this cost model. A genetic algorithm was used to initialize and modify a population of designs successively producing better and better designs. The blade element momentum theory was used for aerodynamic analysis of each design. Airfoils and polar data were taken from the Low Speed Airfoil Tests conducted at UIUC (Michael Selig, 2024). Structural analysis was rudimentary with the blade treated as a beam in static bending.

The results of the optimization were encouraging. A cost of energy of 0.67 $/Kwh was obtained for the optimized design which was less than that of the benchmark Skystream 3.7 wind turbine. The resulting blade was slender as would be expected from the double incentive of maximization of power extraction and minimization of volume. The obtained coefficient of power of 0.362 was also found to be above that of the benchmark even though aerodynamics was not the primary objective. This illustrates the utility of the cost of energy objective which improves the aerodynamic performance of the optimized turbine while lowering the cost.

The main limitation of this research is the absence of a robust structural analysis scheme. This is essential as the objective used tends to make the blade slender and structurally compromised. Fatigue loads, centrifugal loads, critical speed, yawing loads, etc must be included in different load cases with appropriate combinations. Another limitation of this research is the absence of stall data.

The approximation used underestimates the airfoils' performances for a conservative design. In addition, sensitivity analysis revealed that a detailed component cost modeling as well as optimization of the code to run faster to accommodate a larger number of blade elements is warranted.

Future works can tackle the problems mentioned above. In addition, investigating different materials, 3d printing technologies, and print settings and their effect on the optimized design is another potential area of research. It is also noteworthy that the blades comprise a small portion of the cost of small wind turbines. For this reason, a holistic optimization of the entire turbine is sure to give a better cost of energy.

# References


1. Akbari, V., Naghashzadegan, M., Kouhikamali, R., Afsharpanah, F., & Yaïci, W. (2022). Multi-Objective Optimization of a Small Horizontal-Axis Wind Turbine Blade for Generating the Maximum Startup Torque at Low Wind Speeds. *Machines*, *10*(9), 785. https://doi.org/10.3390/machines10090785
2. Akour, S. N., Al-Heymari, M., Ahmed, T., & Khalil, K. A. (2018). Experimental and theoretical investigation of micro wind turbine for low wind speed regions. *Renewable Energy*, *116*, 215–223. https://doi.org/10.1016/j.renene.2017.09.076
3. Alexander, P., Allen, S., & Dutta, D. (1998). Part orientation and build cost determination in layered manufacturing. *Computer-Aided Design*, *30*(5), 343–356. https://doi.org/10.1016/S0010-4485(97)00083-3
4. Andrew Ning, S., Damiani, R., & Moriarty, P. J. (2014). Objectives and Constraints for Wind Turbine Optimization. *Journal of Solar Energy Engineering*, *136*(4), 041010. https://doi.org/10.1115/1.4027693
5. Bassett, K., Carriveau, R., & Ting, D. S.-K. (2015). 3D printed wind turbines part 1: Design considerations and rapid manufacture potential. *Sustainable Energy Technologies and Assessments*, *11*, 186–193. https://doi.org/10.1016/j.seta.2015.01.002
6. Bekele, G., & Palm, B. (2009). Wind energy potential assessment at four typical locations in Ethiopia. *Applied Energy*, *86*(3), 388–396. https://doi.org/10.1016/j.apenergy.2008.05.012
7. Bernard, A., Monzón, M., & Pei, E. (Eds.). (2019). *Additive Manufacturing—Developments in Training and Education* (1st ed. 2019). Springer International Publishing : Imprint: Springer. https://doi.org/10.1007/978-3-319-76084-1
8. Busachi, A., Erkoyuncu, J., Colegrove, P., Martina, F., Watts, C., & Drake, R. (2017). A review of Additive Manufacturing technology and Cost Estimation techniques for the defence sector. *CIRP Journal of Manufacturing Science and Technology*, *19*, 117–128. https://doi.org/10.1016/j.cirpj.2017.07.001
9. Carriveau, R. (Ed.). (2011). *Fundamental and Advanced Topics in Wind Power*. InTech. https://doi.org/10.5772/731

10. Chehouri, A., Younes, R., Ilinca, A., & Perron, J. (2015). Review of performance optimization techniques applied to wind turbines. *Applied Energy*, *142*, 361–388. https://doi.org/10.1016/j.apenergy.2014.12.043
11. Clifton-Smith, M. J. (2009). Wind Turbine Blade Optimisation with Tip Loss Corrections. *Wind Engineering*, *33*(5), 477–496. https://doi.org/10.1260/030952409790291226
12. Costabile, G., Fera, M., Fruggiero, F., Lambiase, A., & Pham, D. (2017). Cost models of additive manufacturing: A literature review. *International Journal of Industrial Engineering Computations*, 263–283. https://doi.org/10.5267/j.ijiec.2016.9.001
13. Ding, J., Baumers, M., Clark, E. A., & Wildman, R. D. (2021). The economics of additive manufacturing: Towards a general cost model including process failure. *International Journal of Production Economics*, *237*, 108087. https://doi.org/10.1016/j.ijpe.2021.108087
14. Dingeto Hailu, A., Kalbessa Kumsa, D., & Department of Mechanical Engineering, Bule Hora University (BHU), Ethiopia, P. O. Box 144. (2021). Ethiopia renewable energy potentials and current state. *AIMS Energy*, *9*(1), 1–14. https://doi.org/10.3934/energy.2021001
15. Djairam, D., Hubacz, A. N., Morshuis, P. H. F., Marijnisen, J. C. M., & Smit, J. J. (2005). The development of an electrostatic wind energy converter (EWICON). *2005 International Conference on Future Power Systems*, 4 pp. – 4. https://doi.org/10.1109/FPS.2005.204208
16. Eales, A., Leary, J., & Latoufis, K. (2016). *Market Assessment for Locally Manufactured Small Wind Turbines in Ethiopia*. https://doi.org/10.13140/RG.2.2.15613.61922
17. Energy Institute. (2023). *Resources and data downloads*. Statistical Review of World Energy. https://www.energyinst.org/statistical-review/resources-and-data-downloads
18. *Energy Profile Ethiopia* (p. 4). (2023). International Renewable Energy Agency. https://www.irena.org/-/media/Files/IRENA/Agency/Statistics/Statistical_Profiles/Africa/Ethiopia_Africa_RE_SP.pdf
19. *Ethiopia—Multi-Tier Framework (MTF) Survey | Data Catalog*. (n.d.). Retrieved June 13, 2023, from https://datacatalog.worldbank.org/search/dataset/0041725

20. Fuglsang, P., Bak, C., Schepers, J. G., Bulder, B., Cockerill, T. T., Claiden, P., Olesen, A., & Van Rossen, R. (2002). Site-specific Design Optimization of Wind Turbines. *Wind Energy*, *5*(4), 261–279. https://doi.org/10.1002/we.61
21. Gigue`re, P., & Selig, M. S. (1998). New Airfoils for Small Horizontal Axis Wind Turbines. *Journal of Solar Energy Engineering*, *120*(2), 108–114. https://doi.org/10.1115/1.2888052
22. Gipe, P., & Möllerström, E. (2022). An overview of the history of wind turbine development: Part I—The early wind turbines until the 1960s. *Wind Engineering*, *46*(6), 1973–2004. https://doi.org/10.1177/0309524X221117825
23. Gipe, P., & Möllerström, E. (2023). An overview of the history of wind turbine development: Part II–The 1970s onward. *Wind Engineering*, *47*(1), 220–248. https://doi.org/10.1177/0309524X221122594
24. Hau, E., & Hau, E. (2006). *Wind turbines: Fundamentals, technologies, application, economics* (2nd [English] ed). Springer.
25. *ILOSTAT Data Explorer*. (n.d.). Retrieved August 3, 2024, from https://rshiny.ilo.org/dataexplorer31/?region=AFRICA&lang=en&id=ETH_A
26. Kadir, A. Z. A., Yusof, Y., & Wahab, M. S. (2020). Additive manufacturing cost estimation models—A classification review. *The International Journal of Advanced Manufacturing Technology*, *107*(9–10), 4033–4053. https://doi.org/10.1007/s00170-020-05262-5
27. Lyon, C. A. (Ed.). (1997). *Summary of low speed airfoil data. 3 / Christopher A. Lyon* (1. print). SoarTech Publications.
28. Maki, K., Sbragio, R., & Vlahopoulos, N. (2012). System design of a wind turbine using a multi-level optimization approach. *Renewable Energy*, *43*, 101–110. https://doi.org/10.1016/j.renene.2011.11.027
29. Mazumdar, S. K. (2002). *Composites manufacturing: Materials, product, and process engineering*. CRC Press.
30. Michael Selig. (2024). *UIUC APA - LSATs*. https://m-selig.ae.illinois.edu/uiuc_lsat.html
31. Ministry of Water, Irrigation, and Energy. (2019). *National Electrification Program 2.0*. Ministry of Water, Irrigation, and Energy.

https://www.powermag.com/wp-content/uploads/2020/08/ethiopia-national-electrification-program.pdf

32. NEA. (2020). *Projected Costs of Generating Electricity—2020 Edition*. OECD Publishing. https://www.oecd-nea.org/jcms/pl_51110/projected-costs-of-generating-electricity-2020-edition?id=pl_51110&preview=true
33. Novaes Menezes, E. J., Araújo, A. M., & Bouchonneau Da Silva, N. S. (2018). A review on wind turbine control and its associated methods. *Journal of Cleaner Production*, *174*, 945–953. https://doi.org/10.1016/j.jclepro.2017.10.297
34. Polinder, H., Ferreira, J. A., Jensen, B. B., Abrahamsen, A. B., Atallah, K., & McMahon, R. A. (2013). Trends in Wind Turbine Generator Systems. *IEEE Journal of Emerging and Selected Topics in Power Electronics*, *1*(3), 174–185. https://doi.org/10.1109/JESTPE.2013.2280428
35. Poole, S., & Phillips, R. (2015). Rapid prototyping of small wind turbine blades using additive manufacturing. *2015 Pattern Recognition Association of South Africa and Robotics and Mechatronics International Conference (PRASA-RobMech)*, 189–194. https://doi.org/10.1109/RoboMech.2015.7359521
36. Post, B. K., Chesser, P. C., Roschli, A. C., Love, L. J., & Gaul, K. T. (2018). *Large-Scale Additive Manufacturing for Low Cost Small-Scale Wind Turbine Manufacturing* (ORNL/TM--2018/1015, 1493993; p. ORNL/TM--2018/1015, 1493993). https://doi.org/10.2172/1493993
37. Post, B., Richardson, B., Lind, R., Love, L., Lloyd, P., Kunc, V., Rhyne, B. J., Roschli, A., Hannan, J., Nolet, S., Veloso, K., & Kurup, P. (2017). *BIG AREA ADDITIVE MANUFACTURING APPLICATION IN WIND TURBINE MOLDS*. https://www.semanticscholar.org/paper/BIG-AREA-ADDITIVE-MANUFACTURING-APPLICATION-IN-WIND-Post-Richardson/e9f68c88ee6babdb14ede590f95c9c3829f2f836
38. *Power Generation – eep*. (n.d.). Retrieved October 6, 2023, from https://www.eep.com.et/en/power-generation/

39. *Renewable Power Remains Cost-Competitive amid Fossil Fuel Crisis*. (2022, July 13). https://www.irena.org/news/pressreleases/2022/Jul/Renewable-Power-Remains-Cost-Competitive-amid-Fossil-Fuel-Crisis
40. Ritchie, H., Roser, M., & Rosado, P. (2022). Energy. *Our World in Data*. https://ourworldindata.org/energy-production-consumption
41. Sale, D. C. (2010). HARP_Opt User's Guide. *NWTC Design Codes*.
42. Selig, M. S. (Ed.). (1995). *Summary of low speed airfoil data*. SoarTech Publications.
43. Selig, M. S., & Coverstone-Carroll, V. L. (1996). Application of a Genetic Algorithm to Wind Turbine Design. *Journal of Energy Resources Technology*, *118*(1), 22–28. https://doi.org/10.1115/1.2792688
44. *Small Turbine Product Reviews*. (n.d.). WIND WORKS. Retrieved August 5, 2024, from https://wind-works.org/category/small-turbine-product-reviews/
45. Stehly, T., Duffy, P., & Mulas Hernando, D. (2023). *2022 Cost of Wind Energy Review [Slides]* (NREL/PR--5000-88335, 2278805, MainId:89111; p. NREL/PR--5000-88335, 2278805, MainId:89111). https://doi.org/10.2172/2278805
46. Tandel, R., Shah, S., & Tripathi, S. (2021). A state-of-art review on Bladeless Wind Turbine. *Journal of Physics: Conference Series*, *1950*(1), 012058. https://doi.org/10.1088/1742-6596/1950/1/012058
47. Tummala, A., Velamati, R. K., Sinha, D. K., Indraja, V., & Krishna, V. H. (2016). A review on small scale wind turbines. *Renewable and Sustainable Energy Reviews*, *56*, 1351–1371. https://doi.org/10.1016/j.rser.2015.12.027
48. Tzen, E. (2020). Small wind turbines for on grid and off grid applications. *IOP Conference Series: Earth and Environmental Science*, *410*(1), 012047. https://doi.org/10.1088/1755-1315/410/1/012047
49. Vimmerstedt, L., Stehly, T., Akar, S., Sekar, A., Mirletz, B., Stright, D., Augustine, C., Beiter, P., Bhaskar, P., Blair, N., Cohen, S., Cole, W., Duffy, P., Feldman, D., Gagnon, P., Kurup, P., Murphy, C., Ramasamy, V., Robins, J., … Hoffmann, J. (2022). *2022 Annual Technology Baseline (ATB) Cost and Performance Data for Electricity Generation*

*Technologies* (p. 13 files) [Dataset]. DOE Open Energy Data Initiative (OEDI); National Renewable Energy Laboratory (NREL). https://doi.org/10.25984/1871952

50. Westwood, R. (2012). *Seismic monitoring and multiphysics modelling of ground-borne vibrations from small wind turbines* [PhD Thesis].
51. *Wind Turbines*. (n.d.). Retrieved June 10, 2024, from http://www.windmeasurementinternational.com/wind-turbines/om-turbines.php
52. *Wind Turbines Comparison 2009*. (n.d.). Retrieved August 5, 2024, from http://svig.bertrand-blanc.com/wse/Turbines/index.php
53. *Wind turbines. Part 2, Small wind turbines*. (2013). International Electrotechnical Commission.
54. Wood, D. (2011). *Small wind turbines: Analysis, design, and application*. Springer.
55. *World Bank Open Data*. (n.d.). World Bank Open Data. Retrieved October 11, 2023, from https://data.worldbank.org
56. *XzeresSkystream3.7_2.1kW_3.7—NREL/turbine-models power curve archive 0 documentation*. (n.d.). Retrieved August 5, 2024, from https://nrel.github.io/turbine-models/XzeresSkystream3.7_2.1kW_3.7.html
57. Yurdusev, M. A., Ata, R., & Çetin, N. S. (2006). Assessment of optimum tip speed ratio in wind turbines using artificial neural networks. *Energy*, *31*(12), 2153–2161. https://doi.org/10.1016/j.energy.2005.09.007

# Appendix

## Appendix A: Source code

### Parameters.py

```
from math import pi, log, gamma, sqrt

from json import load


n_el = 20 ## number of blade elements

n_airfoils = 2 ## number of airfoils to use

n_b = 3

rho = 1.225 ## air density

nu = 1e-5 ## kinematic viscosity of air

P_rated = 2400 ## rated power

iters = 1000 ## number of iteration for the genetic algorithm

pop_size = 200 ## population size

mut_rate_i = 0.1 ## initial mutation rate

mut_rate_f = 0.5 ## initial mutation rate

S_yld = 261000000 ## min yield strength for 3D printed PLA with similar print settings

sf = 1.5 ## bending safety factor

l_wb = 4.24 ## weibull scale parameter for the windspeed distribution of Addis Ababa

k_wb= 2.01 ## weibull shape parameter for the windspeed distribution of Addis Ababa

p_aco = 1e-5 ## probability windspeed is above cut-out windspeed

v_ci = 3.5 ## cut-in windspeed

v_co = int(l_wb * (-log(p_aco)) ** (1 / k_wb)) + 1 ## cut-out windspeed

v_m = l_wb * gamma(1 + 1 / k_wb) ## mean windspeed

v_sd = l_wb * sqrt(gamma(1 + 2 / k_wb) - gamma(1 + 1 / k_wb) ** 2)
```

```
tsr_min = 3 ## minimum tip-speed ratio

tsr_max = 9 ## maximum tip-speed ratio

v_opt_min = max(v_ci, v_m - 2 * v_sd)

v_opt_max = min(v_co, v_m + 2 * v_sd)

r_min = sqrt(2 * P_rated / (pi * 0.58 * rho * v_opt_max ** 3))

r_max = sqrt(2 * P_rated / (pi * 0.1 * rho * v_opt_min ** 3))

n_b_v = 20 ## number of velocity buckets

n_var = 3 ## number of design variables

elite_frac = 0.01

c_p_proj = 0.4

k = 180/pi

k_i = pi / 180

k_s = 1e-10 ## stress penalty coefficient

k_tsr = 1

k_alpha = 0.5

pdim_max = 0.2

with open("coefficient_data.json") as f:

    c_data = load(f)

#airfoil_names = list(c_data.keys())

airfoil_names = [['BW-3', 'SG6040'], ['GOE 417A', 'SD7062', 'SG6041', 'SG6042', 'SG6043', 'USNPS-4']]
```

**cost_model.py**

```
def cost_function(vol):

    return vol
```

**windspeed_pd.py**

```
from parameters import *

from math import exp


def get_probability(V_1, V_2):

    Ph = (1 - exp(-(V_2 / l_wb) ** k_wb))

    Pl = (1 - exp(-(V_1 / l_wb) ** k_wb))

    return Ph – Pl
```

**BEM_Re_intrp.py**

```
from math import pi, sqrt, atan2, sin, cos, log, gamma

import numpy as np

import get_airfoil_data

from scipy.optimize import fixed_point, fsolve

from parameters import *

from windspeed_pd import get_probability

from cost_model import cost_function

from random import random

import matplotlib.pyplot as plt


##=============================================================================
=

## coe optimization

def BEM(tsr, v_opt, airfoils):

    cp_list = [None] * n_b_v

    P_list = [None] * n_b_v
```

```
    opt_twists = [None] * n_el
    opt_ch = [None] * n_el
    AEP = 0
    stress_penalty = 0
    vol = 0
    coe = 0
     Ixx, Iyy, Ixy, A_sec, c = [None, None], [None, None], [None, None], [None, None], [None, None]
    Ixx[0], Iyy[0], Ixy[0], A_sec[0], c[0] = c_data[airfoils[0]][-1]
    Ixx[1], Iyy[1], Ixy[1], A_sec[1], c[1] = c_data[airfoils[1]][-1]
    R = sqrt(2 * P_rated / (c_p_proj * pi * rho * v_opt ** 3))
    r_h = 0.1 * R
    invalid_cp = False
    def opt_power_calc(tsr_opt):
        nonlocal opt_twists, opt_ch
        w_opt = tsr_opt * v_opt / R
        P_opt = 0

        for j in range(n_el - 1, -1, -1):
            ## iterating over the blade elements
            dr = (R - r_h) / n_el
            r = r_h + dr / 2 + j * dr ## distance of blade element from rotor axis
            # alpha = alpha_r + j * (alpha_t - alpha_r) / (n_el - 1) ## angle of attack of the airfoil
            airfoil = airfoils[int(n_airfoils * j / n_el)]
            lam_r = tsr_opt * r / R
            ch_av = 0
```

```
alpha, c_l, c_d = 0, 0, 0
a, a_p = 0.3, 0
v_T, v_A = 0, 0
v = v_opt
def Re_calc(var):
    nonlocal v, c_l, c_d, v_A, v_T, a, a_p, alpha, ch_av
    Re = var
    alpha = get_airfoil_data.get_max_ldr_alpha(airfoil, Re)
    c_l, c_d = get_airfoil_data.get_coefficients(airfoil, Re, alpha)
    ch_av = min(2 * sqrt(3) * r_h , 16 * pi / (9 * c_l * n_b * tsr * sqrt(4 / 9 + (lam_r + 2 / (9 * lam_r)) ** 2)))
    sigma = n_b * ch_av / (2 * pi * r)

    def equations1(vars):
        a, a_p = vars
        u_T = sqrt((1 - a) ** 2 + ((1 + a_p) * lam_r) ** 2)
        sinphi = (1 - a) / u_T
        cosphi = ((1 + a_p) * lam_r) / u_T
        if sinphi == 0:
            F = 1
        else:
            F = (2 / pi) * np.arccos(np.exp(-(n_b / 2) * (R - r) / (r * abs(sinphi))))
        c_a = c_l * cosphi + c_d * sinphi
        c_a_p = c_l * sinphi - c_d * cosphi
        a_c = 1 / 3
        if a <= a_c:
```

```
                f_a = a * F * (1 - a * F)
            else: ## hight thrust correction according to clifton-smith
                f_a = (a_c * F) ** 2 + (1 - 2 * a_c * F) * a * F

            return (4 * f_a - u_T ** 2 * sigma * c_a, 4 * a_p * F * (1 - a * F) * lam_r - u_T ** 2 *
sigma * c_a_p)
        sol = fsolve(equations1, (a, a_p))
        a, a_p = sol

        v_A = (1 - a) * v_opt
        v_T = (1 + a_p) * w_opt * r
        v = sqrt(v_A ** 2 + v_T ** 2)
        return Re - ch_av * v / nu

    Re = fsolve(Re_calc, 300000, xtol = 1e-3)

    i = k * atan2(v_T, v_A) ## incidence angle
    twist = alpha + i
    opt_twists[j] = twist
    opt_ch[j] = ch_av
    dA_b = ch_av * dr
    dF_T_opt = 0.5 * rho * dA_b * v * (c_l * v_A - c_d * v_T)
    P_opt += n_b * dF_T_opt * r * w_opt
  return P_opt
P_opt = opt_power_calc(tsr)
if P_opt > P_rated:
```

```
    left_tsr = 0
    right_tsr = tsr
    ctr = 0
    while right_tsr - left_tsr > 0.001 and ctr < 50:
        mid_tsr = (left_tsr + right_tsr) / 2
        P_opt = opt_power_calc(mid_tsr)
        if P_opt == P_rated:
            break
        if P_opt > P_rated:
            right_tsr = mid_tsr
        else:
            left_tsr = mid_tsr
        ctr += 1
    print(P_opt)
for i_v_2 in range(n_b_v):
    temp_stress_penalty = 0
    v_i = v_ci + i_v_2 * (v_co - v_ci) / (n_b_v)
    def power_calc(oper_tsr):
        nonlocal temp_stress_penalty
        w = oper_tsr * v_i / R
        F_T, F_A, M_T, M_A = 0, 0, 0, 0
        s = 0
        A_b = 0
        P = 0
        for j in range(n_el - 1, -1, -1):
```

```
## iterating over the blade elements
dr = (R - r_h) / n_el
r = r_h + dr / 2 + j * dr ## distance of blade element from rotor axis
ch_av = opt_ch[j] ## average chord of the element
 dA_b = ch_av * dr ## d A_b = (R - r) * (ch_1 - ch_n) / n + ch_n * (R - r_h) / n ## blade element area
# alpha = alpha_r + j * (alpha_t - alpha_r) / (n_el - 1) ## angle of attack of the airfoil
airfoil_ind = int(n_airfoils * j / n_el)
airfoil = airfoils[airfoil_ind]
v = v_i
c_l, c_d = 0, 0
opt_twist = opt_twists[j]
v_T, v_A = 0, 0
a, a_p = 0.3, 0
def alpha_calc(var):
    nonlocal v, c_l, c_d, v_A, v_T, a, a_p
    alpha, = var
    Re = ch_av * v / nu
    c_l, c_d = get_airfoil_data.get_coefficients(airfoil, Re, alpha)
    lam_r = w * r / v_i
    sigma = n_b * ch_av / (2 * pi * r)

    def equations2(vars):
        a, a_p = vars
        u_T = sqrt((1 - a) ** 2 + ((1 + a_p) * lam_r) ** 2)
        sinphi = (1 - a) / u_T
```

```
            cosphi = ((1 + a_p) * lam_r)/ u_T
            if sinphi == 0:
                F = 1
            else:
                F = (2 / pi) * np.arccos(np.exp(-(n_b / 2) * (R - r) / (r * abs(sinphi))))
            c_a = c_l * cosphi + c_d * sinphi
            c_a_p = c_l * sinphi - c_d * cosphi
            a_c = 1 / 3

            if a <= a_c:
                f_a = a * F * (1 - a * F)
            else: ## hight thrust correction according to clifton-smith
                f_a = (a_c * F) ** 2 + (1 - 2 * a_c * F) * a * F
            return 4 * f_a - u_T ** 2 * sigma * c_a, 4 * a_p * F * (1 - a * F) * lam_r - u_T ** 2 *
sigma * c_a_p
        sol = fsolve(equations2, (a, a_p))
        a, a_p = sol

        v_A = (1 - a) * v_i
        v_T = (1 + a_p) * w * r
        v = sqrt(v_A ** 2 + v_T ** 2)
        i = k * atan2(v_T, v_A) ## incidence angle
        return alpha - (opt_twist - i)

    alpha = fsolve(alpha_calc, 5)
```

```
            dF_A = 0.5 * rho * dA_b * v * (c_l * v_T + c_d * v_A) ## axial force on the element

            dF_T = 0.5 * rho * dA_b * v * (c_l * v_A - c_d * v_T) ## tangential force on the element

            M_A += (F_A * dr + dF_A * dr / 2) ## moment created by the axial forces from the tip up to that element at the base of the element

            M_T += (F_T * dr + dF_T * dr / 2) ## moment created by the tangential forces from the tip up to that element at the base of the element

            M = sqrt(M_A ** 2 + M_T ** 2)

            F_A += dF_A

            F_T += dF_T

            force_angle = k * atan2(F_A, F_T)

            F = sqrt(F_A ** 2 + F_T ** 2)

            theta = opt_twist - force_angle


             I = ch_av ** 4 * (Ixx[airfoil_ind] * cos(k_i * theta) ** 2 + Iyy[airfoil_ind] * sin(k_i * theta) ** 2 + 2 * Ixy[airfoil_ind] * sin(k_i * theta) * cos(k_i * theta))

            c_el = c[airfoil_ind] * ch_av

            A_sec_el = A_sec[airfoil_ind] * ch_av ** 2

            dP = dF_T * r * w ## power per element

            P += (n_b * dP) ## summing up the power from each element on all blades

            s = sqrt((M * c_el / I) ** 2 + 3 * (F / A_sec_el) ** 2)

            temp_stress_penalty += int(s > (S_yld / sf)) * ((s - S_yld / sf) / S_yld) ** 2

        return P

    P = power_calc(tsr)

    if P > P_rated:

        P = P_rated

    if P < 0:
```

```
            AEP = 0
            break
        c_p = P / (0.5 * rho * pi * (R ** 2) * (v_i ** 3))
        stress_penalty += temp_stress_penalty
        if c_p > 0.593:
            invalid_cp = True
            print(f"Invalid c_p. c_p = {c_p}, ideal_tsr = {tsr}, P = {P}.")
        cp_list[i_v_2] = c_p
        P_list[i_v_2] = P
        AEP += get_probability(v_i, v_i + (v_co - v_ci) / (n_b_v)) * P
    AEP *= 8760 * 3600
    for j in range(n_el):
        airfoil_ind = int(n_airfoils * j / n_el)
        vol += n_b * A_sec[airfoil_ind] * (opt_ch[j] ** 2) * (R - r_h) / n_el
    if invalid_cp:
        AEP = 0
    if AEP > 1:
        coe = cost_function(vol) / AEP
    else:
        coe = cost_function(vol) * (abs(AEP) + 1)
    return coe, vol, AEP, stress_penalty, P_list, opt_twists, cp_list, opt_ch, R
```

**Config.py**

```
import random
from BEM_Re_intrp import BEM
from numpy import tan, pi, sqrt
```

```
from parameters import *


class Config:
    def __init__(self, tsr = 0, airfoils = [], v_opt = 0, R = 0):
        self.tsr = tsr
        self.airfoils = airfoils
        self.raw_fitness = 0
        self.fitness = 0
        self.stress_penalty = 0
        self.twist_angles = []
        self.coe = 0
        self.volume = 0
        self.AEP = 0
        self.radius = R
        self.v_opt = v_opt
        self.P_list = []
        self.cp_list = []
        self.ch = []


    def calc_fitness(self):
        res = BEM(self.tsr, self.v_opt, self.airfoils)
        self.coe, self.volume, self.AEP, self.stress_penalty, self.P_list, self.twist_angles, self.cp_list,
self.ch, self.radius = res
        self.raw_fitness = self.coe + k_s * self.stress_penalty


    def mutate(self, mut_rate):
```

```
        trait_mr = mut_rate / n_var
        for i in range(n_airfoils):
            if random.random() < (trait_mr / n_airfoils):
                self.airfoils[i] = random.choice(airfoil_names[i])
        if random.random() < trait_mr:
            self.v_opt = random.uniform(max(v_ci, v_m - 3 * v_sd), min(v_co, v_m + 3 * v_sd))
        # if random.random() < trait_mr:
         #      self.radius = random.uniform(sqrt(2 * P_rated / (pi * 0.5 * rho * min(v_co, v_m + 2 *
v_sd) ** 3)), sqrt(2 * P_rated / (pi * 0.3 * rho * max(v_ci, v_m - 2 * v_sd) ** 3)))
        if random.random() < trait_mr:
            self.tsr = random.uniform(tsr_min, tsr_max)
```

**Population.py**

```
import random
from config import Config
from parameters import *


class Population:
    def __init__(self, size, mut_rate):
        self.size = size
        self.mut_rate = mut_rate
        self.configs = [None] * size
        self.fittest = None


    def populate(self):
        for i in range(self.size):
```

```
            new_config = Config()
            new_config.airfoils = [None] * n_airfoils
            new_config.mutate(n_var * n_airfoils)
            self.configs[i] = new_config

    def crossover(self, configA: Config, configB: Config) -> Config:
        airfoils_c = []
        for i in range(n_airfoils):
            airfoils_c.append(random.choice([configA, configB]).airfoils[i])

            v_opt_c_temp = configA.v_opt + ((v_opt_max - v_opt_min) * int(configB.v_opt < configA.v_opt) - (configA.v_opt - configB.v_opt)) / 2
        v_opt_c =  v_opt_c_temp - (v_opt_max - v_opt_min) * int(v_opt_c_temp > v_opt_max)

        tsr_c_temp = configA.tsr + ((tsr_max - tsr_min) * int(configB.tsr < configA.tsr) - (configA.tsr - configB.tsr)) / 2
        tsr_c =  tsr_c_temp - (tsr_max - tsr_min) * int(tsr_c_temp > tsr_max)

        # r_c_temp = configA.radius + ((r_max - r_min) * int(configB.radius < configA.radius) - (configA.radius - configB.radius)) / 2
        # r_c =  r_c_temp - (r_max - r_min) * int(r_c_temp > r_max)

        child = Config(tsr_c, airfoils_c, v_opt_c)
        child.mutate(self.mut_rate)
        return child
    def get_fitness(self, config):
```

```
        return config.raw_fitness
    def calc_fitness_all(self):
        min_fitness = float("Inf")
        max_fitness = float("-Inf")
        print("Calculating fitness...")
        for config in self.configs:
            config.calc_fitness()
            if config.raw_fitness > max_fitness:
                max_fitness = config.raw_fitness
            if config.raw_fitness < min_fitness:
                min_fitness = config.raw_fitness
                self.fittest = config
        for config in self.configs:
            if max_fitness == min_fitness:
                config.fitness = 0.5
            else:
                    config.fitness = (log(max_fitness) - log(config.raw_fitness)) / (log(max_fitness) -
log(min_fitness))
        self.configs = sorted(self.configs, key = self.get_fitness)
```

**Main.py**

```
from population import Population
from parameters import *
import random
import matplotlib.pyplot as plt
from time import time, localtime
```

```
import copy


def main():
    global c_p_proj
    mut_rate = mut_rate_i
    pop = Population(pop_size, mut_rate)
    pop.populate()
    min_obj = [None] * iters
    for i in range(1, iters):
        print(f"This is iteration #{i}.")
        pop.calc_fitness_all()
        c_p_proj = max(pop.fittest.cp_list)
        min_obj[i - 1] = pop.fittest.raw_fitness
        print(f"The coefficient of power for radius calculation for the next generation is {c_p_proj}. Attributes of the best design of this generation are")
        res_dict = pop.fittest.__dict__
        for key in res_dict.keys():
            print(f"{key} = {res_dict[key]}")
        if i == iters // 2:
            mut_rate = mut_rate_f
        new_pop = Population(pop_size, mut_rate)
        print("Creating the next generation...")
        n_elites = 1 + int(elite_frac * pop.size)
        new_pop.configs[:n_elites] = pop.configs[:n_elites]
        for j in range(n_elites, pop.size):
            parentA = None
```

```
            parentB = None
            while parentA is None:
                candidate = random.choice(pop.configs)
                if random.random() < candidate.fitness:
                    parentA = candidate
            while parentB is None:
                candidate = random.choice(pop.configs)
                if random.random() < candidate.fitness:
                    parentB = candidate
            new_pop.configs[j] = pop.crossover(parentA, parentB)
        pop = copy.deepcopy(new_pop)
    print(f"This is iter number {iters}.")
    pop.calc_fitness_all()
    min_obj[iters - 1] = pop.fittest.raw_fitness
    res_dict = pop.fittest.__dict__
    for key in res_dict.keys():
        print(f"{key} = {res_dict[key]}")
    tstruct = localtime(time())
            tstr = "_".join([str(tstruct.tm_year), str(tstruct.tm_mon), str(tstruct.tm_mday),
str(tstruct.tm_hour), str(tstruct.tm_min), str(tstruct.tm_sec)])
    with open("results/result_" + tstr + ".txt", "w+") as f:
        f.write("Pop size" + "\t" + str(pop.size) + "\n")
        f.write("Iters" + "\t" + str(iters) + "\n")
        f.write("Fittest configuration\n")
        for attr in res_dict.keys():
            f.write(attr + "\t" + str(res_dict[attr]) + "\n")
```

```
        for i in range(len(pop.configs)):
            f.write(f"Configuration {i + 1}\n")
            for attr in pop.configs[i].__dict__.keys():
                f.write(attr + "\t" + str(pop.configs[i].__dict__[attr]) + "\n")

    windspeeds = [v_ci + i_v * (v_co - v_ci) / (n_b_v) for i_v in range(n_b_v)]
    plt.figure(0)
    plt.plot(windspeeds, pop.fittest.P_list)
    plt.figure(1)
    plt.plot(range(iters), min_obj)
    plt.show()

if __name__ == "__main__":
    main()
```